STAR-RIS Assisted Secure Transmission for Downlink Multi-Carrier NOMA Networks

Yanbo Zhang, Zheng Yang, Jingjing Cui, Peng Xu, Gaojie Chen, Yi Wu, Marco Di Renzo

STAR-RIS Assisted Secure Transmission for Downlink Multi-Carrier NOMA Networks

Yanbo Zhang, Zheng Yang, *Member, IEEE*, Jingjing Cui, *Senior Member, IEEE*, Peng Xu, *Member, IEEE*, Gaojie Chen, *Senior Member, IEEE*, Yi Wu, *Member, IEEE*, and Marco Di Renzo, *Fellow, IEEE*

***Abstract*— This paper investigates the secrecy performance for simultaneously transmitting and reflecting reconfigurable intelligent surface (STAR-RIS) assisted downlink multi-carrier non-orthogonal multiple access (NOMA) networks, consisting of multiple legitimate users and eavesdroppers. We propose two STAR-RIS-NOMA schemes for maximizing the secrecy performance by jointly optimizing the transmission and reflection beamforming of the STAR-RIS, the transmit beamforming of the base station (BS), the power allocation coefficients and the user pairing vector under the full channel state information (CSI) and the statistical CSI of the eavesdropping channel, respectively. For the full CSI available to the BS, an alternating beamforming algorithm is proposed for maximizing the secrecy sum rate. Specifically, we first propose a user pairing scheme based on the differences of user's channel gains. Then the beamforming vectors and the power allocation coefficients are optimized based on the techniques of semidefinite programming and surrogate lower bound approximation, respectively. For the statistical CSI available to the BS, the problem of minimizing the maximum secrecy outage probability (SOP) is investigated. By invoking the subroutines of alternating beamforming algorithm, we first derive an exact SOP given the user pairing. Then, we conceive the beamforming vectors and the power allocation coefficients by linear matrix inequality and linear programming, respectively. Simulation results show that: 1) the secrecy performance of the proposed STAR-RIS-NOMA scheme outperforms the existing conventional RIS-NOMA scheme and RIS assisted orthogonal multiple access (RIS-OMA) scheme; 2) the proposed alternating beamforming algorithm is capable of achieving a near-optimal performance with low complexity compared to the exhaustive search.**

***Index Terms*— Secrecy performance, simultaneously transmitting and reflecting reconfigurable intelligent surface (STAR-RIS), non-orthogonal multiple access (NOMA), user pairing, alternating beamforming.**

I. Introduction

IN THE upcoming sixth-generation (6G) era, the demands for high-data-rate and low latency will exponentially increase and the resulting demands for novel wireless transmission technologies become more and more urgent [1], [2]. Reconfigurable intelligent surface (RIS) has been considered as a promising candidate technology for enabling 6G wireless communications, since it can be realized with low cost, low energy consumption, and high reliability [3], [4]. Generally, RIS contains a large number of low-cost reconfigurable passive elements. The RIS can control smart radio environments (SRE) proactively by intelligently adjusting the amplitudes and phase shifts of the elements [5]. Furthermore, non-orthogonal multiple access (NOMA) technology has the advantages of high spectrum efficiency and massive connectivity [6]. In particular, NOMA is capable of outperforming conventional orthogonal multiple access (OMA) techniques, since multiple users can be served at the same time/freqency/code resource with the power domain multiplexing at the transmitter [7]. Therefore, NOMA is considered as a promising technique for future resource constrained mobile networks. Given the appealing characteristics of RIS and NOMA, the combination of the two techniques would introduce a win-win option [8], [9].

Most of the existing work on RIS-NOMA focuses on conventional RIS (C-RIS) reflecting incident signals only [10], [11], which requires that the transmitters are located at the same side as the receivers. This half-space SRE coverage, limits the flexibility and coverage ranges of RIS [12]. To address this issue, a new type of block array, namely, simultaneous transmitting and reflecting RIS (STAR-RIS) [13], and intelligent omni-surfaces [14], is proposed. Different from reflecting-only C-RIS, STAR-RIS has independently adjustable surface's electrical impedance and magnetic impedance [15], which facilitates to control the amplitudes and phase shifts of transmitted and reflected signals. In addition to inheriting the beneficial features of reflecting-only C-RIS-NOMA, STAR-RIS-NOMA have the following unique advantages [16], [17]: 1) given the simultaneous control of transmitted and reflected signals, STAR-RIS-NOMA is capable of providing a full-space SRE coverage, and supporting more users than C-RIS-NOMA; 2) STAR-RIS-NOMA can also provide more degrees-of-

Yanbo Zhang, Zheng Yang, and Yi Wu are with the Fujian Provincial Engineering Technology Research Center of Photoelectric Sensing Application, Key Laboratory of Optoelectronic Science and Technology for Medicine of Ministry of Education, Fujian Normal University, Fuzhou 350007, China (e-mail: zhangybfj@163.com; zyfjnu@163.com; wuyi@fjnu.edu.cn).

Jingjing Cui is with the School of Electronics and Computer Science, University of Southampton, SO17 1BJ Southampton, U.K. (e-mail: jingj.cui@soton.ac.uk).

Peng Xu is with the Chongqing Key Laboratory of Mobile Communications Technology, Chongqing University of Posts and Telecommunications, Chongqing 400065, China (e-mail: xupeng@cqupt.edu.cn).

Gaojie Chen is with the 5GIC & 6GIC, Institute for Communication Systems, University of Surrey, GU2 7XH Guildford, U.K. (e-mail: gaojie.chen@surrey.ac.uk).

Marco Di Renzo is with the Universite Paris-Saclay, CNRS, CentraleSupelec, Laboratoire des Signaux et Systemes, 91192 Gif-sur-Yvette, France (e-mail: marco.di-renzo@universite-paris-saclay.fr).

freedoms (DoFs) than C-RIS-NOMA for system design, which further enhances the spectral efficiency by mitigating the co-channel interference of NOMA networks.

Due to the broadcast nature and vulnerability of wireless channels [18], secure transmission is still one of the challenging issues in 6G networks. To ensure secure transmission, the legitimate users are required to maintain better channel conditions than that of the eavesdroppers [19]. To this end, due to the characteristics of RIS that can adjust the wireless channel, the integration of RIS and physical layer security (PLS) becomes appealing [20], [21]. Specifically, the RIS can modify the wireless channel to achieve the energy enhancement in the legitimate users direction by intelligently adjusting the amplitudes and phase shifts of the passive components, while degrading the information leakage to the eavesdroppers. However, with the increasing coverage of service users, C-RIS can not support the secure transmission in some scenarios. For example, multiple legitimate users and potential eavesdroppers (PEs) are distributed on both sides of C-RIS. In this context, performing secure transmission becomes challenging, since there are always some legitimate users and PEs which are not supported by the C-RIS. To overcome this drawback, STAR-RIS assisted PLS has been developed to achieve secure communication in a full-space manner [22], [23].

Driven by STAR-RIS-NOMA networks, the purpose of this paper is to investigate promising applications of STAR-RIS assisted secure transmission in NOMA networks for further secrecy performance improvement.

A. Related Works

The secrecy rate maximization problem of RIS assisted unmanned aerial vehicle networks was investigated in [24]. The authors of [25] proposed an RIS assisted secure cooperative networks in the presence of a PE, where the buffer-aided relay selection and the RIS reflection coefficients were jointly optimized for maximizing either the average secrecy rate with a delay constraint or the throughput with both delay and secrecy constraints. In [26], the authors proposed an aerial RIS-assisted secure transmission design scheme for air-ground wireless networks, to maximize the sum secrecy rate, where the hovering position of unmanned aerial vehicle (UAV), the transmit beamforming of access point and the phase shifts of RIS were jointly optimized. The authors of [27] proposed an RIS-assisted UAV network for maximizing the average secrecy rate of legitimate user, where the trajectory of UAV, the transmit beamforming and the phase shift of RIS were jointly optimized. In [28], the authors proposed a deep reinforcement learning based secure beamforming scheme for maximizing the secrecy rate of RIS assisted wireless communication networks. Furthermore, RIS can also coexist with existing NOMA networks for further improving secrecy performance [29], [30], [31], [32], [33]. Specifically, the authors of [29] proposed an RIS-NOMA scheme to mitigate the internal and external eavesdropping, which demonstrated that the system secrecy perfrmance can be enhanced by increasing the number of reflecting elements of the RIS or the transmit antennas of the BS. In [30], the secrecy outage probability (SOP) of RIS-NOMA networks was studied, which illustrated that the RIS can significantly improve the secrecy performance of NOMA networks. The authors of [31] proposed an artificial jamming assisted downlink RIS-NOMA network for maximizing the sum rate of legitimate users. In order to combat the security hazards caused by 360° eavesdropping, the authors of [32] studied the secure transmission problem in STAR-RIS assisted uplink NOMA networks, in which the adaptive rate wiretap code and constant rate wiretap code were proposed for maximizing the minimum secrecy capacity and minimizing the maximum SOP, respectively. In [33], the optimization problem of maximizing the secrecy sum rate (SSR) in artificial jamming assisted STAR-RIS-NOMA networks was investigated, where the eavesdropping channel state information (CSI) is available at the BS.

B. Motivations and Contributions

For the secrecy performance of the STAR-RIS assisted NOMA networks, a simplified secure transmission scenario was considered in [32] and [33], where there is one legitimate user on each side of the STAR-RIS. However, there are usually numerous legitimate users and PEs in practical communication environments, which makes STAR-RIS-NOMA networks become complex. On the one hand, in order to exploit the full secrecy potential of STAR-RIS, the resource allocation at the BS, and the transmission and reflection coefficients at the STAR-RIS need to be jointly optimized. However, as the number of legitimate users and PEs increases, solving this joint optimization problem will become more complicated. On the other hand, the complexity of the successive interference cancellation (SIC) of NOMA increases significantly as the number of legitimate users and PEs increases. One efficient method for reducing the complexity was to employ multi-carrier based NOMA techniques [17]. Due to the uncertainty of the legitimate users'channels in multi-carrier transmissions, designing optimal resource allocation becomes a non-trivial task for improving the secrecy performance of STAR-RIS-NOMA networks. In light of the above considerations, we focus on the secure communication of STAR-RIS assisted downlink multi-carrier NOMA networks consisting of multiple legitimate users and PEs. The main contributions of this paper are summarized as follows:

- We consider a downlink multi-carrier STAR-RIS-NOMA secure communication network in the presence of multiple legitimate users and PEs, where the BS sends the superimposed information in each sub-carrier to the corresponding sub-carrier through the transmission/reflection links provided by STAR-RIS. Depending on the availability of eavesdropping CSI, full eavesdropping CSI and statistical eavesdropping CSI are considered. Accordingly, we respectively formulate the SSR maximization problem and the maximum SOP minimization problem subject to each legitimate user's quality of service (QoS) requirements and the BS with the maximal transmit power constraint, both of which are mixed-integer optimization probems.
- For the full eavesdropping CSI, we propose an alternating beamforming algorithm by decomposing the original SSR maximization problem into three subproblems. Specifically, we develop a Kuhn-Munkres (KM) algorithm to solve the user pairing subproblem. Given the user pairing vector, we apply the semidefinite programming (SDP) and successive convex approximation (SCA) techniques for obtaining the transmission and reflection beamforming vectors and transmit beamforming vectors. Finally,

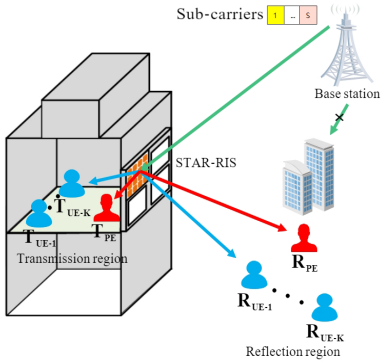

Fig. 1. A STAR-RIS assisted downlink multi-carrier NOMA system model for multiple legitimate users (UEs) and two potential eavesdroppers (PEs).

the power allocation coefficients are obtained using the surrogate lower bound (SLB) approximation.

- For the statistical eavesdropping CSI, an alternating beamforming algorithm is proposed to slove the maximum SOP minimization problem. Firstly, we derive the exact SOP by fixing the user pairing. Then, the non-convex constraints in the joint beamforming optimization subproblem are reformulated into linear matrix inequality (LMI). Furthermore, the subproblem of power allocation is reformulated as a linear programming, which can be solved optimally.
- Simulation results show the convergence of the proposed algorithms and draw two insights. 1) the proposed STAR-RIS-NOMA scheme has secrecy advantage compared with the existing the C-RIS-NOMA scheme and the C-RIS-OMA scheme. This is because STAR-RIS can provide more DoFs than C-RIS for system secrecy designs; 2) the proposed alternating beamforming algorithm can achieve nearly the same secrecy performance as the exhaustive search matching.

C. Organizations and Notations

The rest of this paper is organized as follows. In Section II, the system model is presented. In Section III, the problem formulation of the two STAR-RIS-NOMA schemes are proposed. Section IV develops an alternating beamforming algorithm for the SSR maximization problem under the full CSI of the PE's channel. In Section V, the extended alternating beamforming algorithm is proposed for the maximum SOP minimization problem under the statistical CSI of the PE's channel. Simulation results are presented in Section VI. Finally, the conclusion is drawn in Section VII.

Notation: We adopt boldface capital and lower case letters to denote matrices and vectors, respectively. $\mathbf{W}^H$, Tr($\mathbf{W}$), and Rank($\mathbf{W}$) represent the Hermitian transpose, trace, and rank of the matrix $\mathbf{W}$, respectively. $\mathbf{W} \succeq 0$ means that $\mathbf{W}$ is a positive semidefinite matrix. The (m, n)th element of a matrix $\mathbf{W}$ is denoted by $\mathbf{W}(m, n)$. $\|\mathbf{W}\|_F$ denotes the Frobenius norm of matrix $\mathbf{W}$. $\|\mathbf{w}\|$ denotes the Euclidean norm of $\mathbf{w}$. Diag($\mathbf{w}$) denotes a diagonal matrix, whose diagonal elements corresponds to the elements in the vector $\mathbf{w}$. $\mathbb{C}^{N\times N}$ denotes the $N \times N$ complex space. $|a|$ denotes the magnitude of a complex number a. $\mathbf{I}_N$ is the $N\times N$ identity matrix. $\mathcal{CN}(0, \sigma^2)$ denotes a complex Gaussian distribution with zero mean and variance σ^2. For the convenience of the readers, a summary of key variables is listed in Table I.

II. System Model

A STAR-RIS assisted downlink multi-carrier NOMA network is shown in Fig. 1, which consists of one BS, one STAR-RIS, multiple legitimate users and two PEs. The direct links between BS and users are assumed negligible due to the presence of obstacles [16], [17]. The BS with N antennas sends the confidential information to multiple single-antenna legitimate users, which are located in the transmission region or the reflection region with the aid of the STAR-RIS deployed on the surface of the windows [23]. Here, the STAR-RIS is composed of M elements operating according to the energy splitting (ES) mode [34]. Specifically, all the elements of the STAR-RIS simultaneously work in two modes, i.e., the transmission (T) mode and the reflection (R) mode.[1] It is assumed that there is a single-antenna PE on each side of the STAR-RIS,[2] which intends to intercept the confidential information from the legitimate users. Let T_{PE} and R_{PE} represent the PE in transmission region and reflection region, respectively.

For the considered STAR-RIS-NOMA network in Fig. 1, the total bandwidth B at the BS is divided into S sub-carriers, denoted as $\mathcal{S} = \{1, 2, ..., S\}$, where each sub-carrier is orthogonal to the others. Furthermore, we assume that each sub-carrier can be occupied by at most two legitimate users from different regions[3] and each legitimate user can occupy at most one sub-carrier. The BS sends the superimposed information in each sub-carrier to the corresponding sub-carrier, and then receiver with the stronger channel eliminate multi-user interference by SIC to obtain the desired signal. We also assume that the number of legitimate users in each regions is K, denoted as $\mathcal{K} = \{1, 2, ..., K\}$. More specifically, the legitimate users located in the transmission region and the reflection region are denoted as $\mathcal{T} = \{T_{UE-1}, ..., T_{UE-K}\}$ and $\mathcal{R} = \{R_{UE-1}, ..., R_{UE-K}\}$, respectively. Therefore, all $2K$

[1]Note that there are three existing operating schemes for STAR-RIS [34]. Specifically, 1) The ES protocol, where all elements of the STAR-RIS simultaneously work in the two modes. 2) The mode switching (MS) protocol, where all elements of the STAR-RIS are separated to two parts, namely, one part with M_t elements working in the T mode, while the other with M_r elements working in the R mode, satisfying $M_t + M_r = M$. 3) The time switching (TS) protocol, where the STAR-RIS switches all elements between the two modes in different orthogonal time durations. Since both the transmission and reflection coefficients of each element can be optimized in the STAR-RIS ES mode, which can achieve higher flexibility than the MS mode and the TS mode [34]. Therefore, to investigate the maximum secrecy performance gain of STAR-RIS, we assume that all elements of the STAR-RIS operating according to the ES mode.

[2]In this paper, the considered network is the outdoor to indoor transmission, we assume that the PEs can only eavesdrop the information of the legitimate users located in the same region and that they are non-colluding [22]. In this scenario, the secrecy performance of legitimate users only depends on the eavesdropping channels located in the same region. In the scenario of colluding eavesdropping, all PEs are capable of combining their signals in an optimal manner to decode the information of legitimate users. In addition, the system model can be extended to multiple PEs on each side of the STAR-RIS. In the scenario of multiple PEs, the secrecy performance of each legitimate user depends on the strongest eavesdropping channels located in the same region, which complicates the solution of the optimization problem. The colluding eavesdropping and multiple PEs scenarios will be investigated in future work notably.

[3]In this paper, we adopt the transmission-reflection (T-R) user pairing scheme. Compared with the same region user pairing scheme, the T-R user pairing scheme has the possibility of further improving the difference of the channel gains. This is because the allocation of amplitudes is dominant and effective for channel reconfiguration, so that the T-R user pairing scheme benefits a lot from channel gain differences that the STAR-RIS provides [17].

TABLE I

SUMMARY OF KEY VARIABLES

Variables	Descriptions
$\mathbf{\Theta}_t/\mathbf{\Theta}_r$	The transmission/reflection coefficient matrix.
$\mathbf{v}_t/\mathbf{v}_r$	The transmission/reflection beamforming vector.
β_t^m/β_r^m	The amplitude of the transmission/reflection coefficient of the mth element.
ϕ_t^m/ϕ_r^m	The phase shift of the transmission/reflection coefficient of the mth element.
M, S, K	The total number of the elements of the STAR -RIS, sub-carriers and each region users, respectively.
$\mathbf{w}_s$	The beamforming vector for sub-carrier s.
$\lambda_{s,i,k}$, $\boldsymbol{\lambda}$	The sub-carrier allocation binary variable of user k in region i and the user pairing vector, respectively.
$\rho_{s,i,k}$, $\boldsymbol{\rho}$	The power allocation coefficient of user k in region i on sub-carrier s and the power allocation coefficient vector, respectively.
$s_{s,i,k}$, $\boldsymbol{s}$	The transmit signal of user k in region i on sub -carrier s and the transmit signal vector, respectively.
$\mathbf{h}_{u,s,i,k}$, $\mathbf{h}_{e,i}$	The channel vectors from the STAR-RIS to user k in region i on sub-carrier s and from the STAR-RIS to the PE in region i, respectively.
$\mathbf{G}_s$	The channel matrix from the BS to the STAR-RIS.
$\psi_{s,i}(k)$	The decoding order index of user k in region i on sub-carrier s.
$r_{u,s,i,k}^{u,s,i,k}$, $r_{u,s,i,k}^{u,s,i',k}$	The SINR for user k in region i to decode user k in region i/i'.
$R_{u,s,i,k}^{u,s,i,k}$, $R_{u,s,i,k}^{u,s,i',k}$	The date rate for user k in region i to decode user k in region i/i'.
$r_{e,s,i,k}$, $R_{e,s,i,k}$	The SINR and the date rate for the PE to decode user k in region i on sub-carrier s, respectively.
$\gamma_{u,s,i,k}$, $R_{u,s,i,k}^{min}$	The SINR threshold and the target rate for user k in region i on sub-carrier s, respectively.
$R_{s,i,k}^{sec}$, $P_{s,i,k}^{SOP}$	The secrecy rate and the SOP for user k in region i on sub-carrier s, respectively.
$\widetilde{R}_{s,i,k}^{sec}$	The target secrecy rate for user k in region i on sub-carrier s.
P_{max}	The total transmit power budget.

legitimate users are divided into S pairs, i.e., $K = S$, which indicates that the number of the sub-carriers is the same as that of the paired NOMA legitimate users.

A. STAR-RIS Model

We assume that all the elements of the STAR-RIS can independently change the phase shifts of the transmitted/reflected signals, where the sum energy of the transmitted and reflected signals satisfy the energy conservation constraint [16], [34]. To facilitate the mathematical description of STAR-RIS, we define the transmission coefficient matrix and reflection coefficient matrix as $\mathbf{\Theta}_t = \text{Diag}\big([\sqrt{\beta_t^1}e^{j\phi_t^1}, ..., \sqrt{\beta_t^M}e^{j\phi_t^M}]\big)$, and $\mathbf{\Theta}_r = \text{Diag}\big([\sqrt{\beta_r^1}e^{j\phi_r^1}, ..., \sqrt{\beta_r^M}e^{j\phi_r^M}]\big)$, respectively, where $\sqrt{\beta_t^m}, \sqrt{\beta_r^m} \in [0,1]$, $\beta_t^m + \beta_r^m = 1$ and $\phi_t^m, \phi_r^m \in [0, 2\pi), m \in \mathcal{M} = \{1, 2, ..., M\}$ denote the amplitude and phase shift responses of the mth element, respectively.

B. Signal Model and Channel Model

For the downlink NOMA scheme, the paired users on each sub-carrier are served at the same resource block [6], [7]. The transmit signal sent by the BS at sub-carrier s can be expressed as

$$\mathbf{x}_s = \mathbf{w}_s\left(\sum_{k=1}^{K}\lambda_{s,t,k}\sqrt{\rho_{s,t,k}}s_{s,t,k} + \sum_{k=1}^{K}\lambda_{s,r,k}\sqrt{\rho_{s,r,k}}s_{s,r,k}\right), \tag{1}$$

where $\mathbf{w}_s \in \mathbb{C}^{N\times 1}, s \in \mathcal{S}$, denotes the beamforming vector for sub-carrier s. Furthermore, $\lambda_{s,i,k}, i \in \mathcal{I} = \{t, r\}, k \in \mathcal{K}$, denotes the binary variable for sub-carrier allocation. Specifically, $\lambda_{s,i,k} = 1$, if the user k in region i is allocated to sub-carrier s, and $\lambda_{s,i,k} = 0$ otherwise. The user pairing vector is denoted as $\boldsymbol{\lambda} = [\lambda_{1,t,1}, ..., \lambda_{S,r,K}]$. Moreover, $\rho_{s,i,k}$, $\rho_{s,t,k} + \rho_{s,r,k} = 1$ and $s_{s,i,k}$ denote the power allocation coefficient and the transmitted signal of user k located in region i on sub-carrier s, respectively. The power allocation coefficient vector and the transmitted signal vector are denoted as $\boldsymbol{\rho} = [\rho_{1,t,1}, ..., \rho_{S,r,K}]$ and $\boldsymbol{s} = [s_{1,t,1}, ..., s_{S,r,K}]$, respectively.

We assume that the CSI of the legitimate channels is available at the BS[4] [17]. Based on (1), the received signal of user k located in region i on sub-carrier s is given by

$$y_{u,s,i,k} = \mathbf{h}_{u,s,i,k}^H\mathbf{\Theta}_i\mathbf{G}_s\mathbf{x}_s + n_{u,s,i,k}, \tag{2}$$

where $\mathbf{h}_{u,s,i,k} \in \mathbb{C}^{M\times 1}$ and $\mathbf{G}_s \in \mathbb{C}^{M\times N}$ denote the quasi-static Rician fading channels from the STAR-RIS to user k in region i on sub-carrier s, and from the BS to the STAR-RIS, respectively. Furthermore, $n_{u,s,i,k} \sim \mathcal{CN}(0, \sigma_k^2\mathbf{I}_N)$ denotes the additive white Gaussian noise (AWGN) at the user k in region i on sub-carrier s.

Based on (1), the received signal at the PE in region i is given by

$$y_{e,s,i,k} = \mathbf{h}_{e,i}^H\mathbf{\Theta}_i\mathbf{G}_s\mathbf{x}_s + n_{e,s,i,k}, \tag{3}$$

where $\mathbf{h}_{e,i} \in \mathbb{C}^{M\times 1}$ denotes the quasi-static Rician fading channel from the STAR-RIS to the PE in region i, $n_{e,s,i,k} \sim \mathcal{CN}(0, \sigma_k^2\mathbf{I}_N)$ denotes the AWGN at the PE in region i. For the PE, we consider two types of eavesdropping CSI assumptions. Specifically, when the PE is an internal wiretap node, i.e., another active user of the STAR-RIS-NOMA networks with frequent and steady interaction with the legitimate nodes, the CSI of the PE's channel can be available at the BS [33]. However, when the PE is an external wiretap node, i.e., a purely passive user of the STAR-RIS-NOMA network without frequent and steady interaction with the legitimate nodes, only the statistical CSI of the PE's channel can be available at the BS [36].

III. PROBLEM FORMULATION

In this section, we discuss the security metrics of the considered STAR-RIS-NOMA networks. Then, we consider two secure transmission schemes for the STAR-RIS assisted downlink multi-carrier NOMA networks with respect to the full CSI and the statistical CSI of the PE's channel, respectively.

A. Security Metrics

For the downlink NOMA scheme, the SIC is carried out at the users to eliminate the multi-access interference, and the optimal SIC decoding order depends on users' channel gains [7]. However, for the considered STAR-RIS-NOMA

[4]To characterize the secrecy performance of legitimate users, we assume that the full CSI of the legitimate channels is available at the BS. However, the acquisition of full CSI in STAR-RIS aided communication systems is a challenging task due to the lack of signal processing capabilities for a passive surface. The channel estimation design for STAR-RIS under the ES mode has been studied in [35], and we will focus on the statistical CSI based phase shift design in future research.

networks, the SIC decoding order of each sub-carrier not only depends on the power allocation coefficients $\{\rho_{s,i,k}\}$, but also on the STAR-RIS transmission/reflection matrix $\{\mathbf{\Theta}_i\}$. To facilitate the optimization of the SIC decoding order, let $\psi_{s,i}(k)$ denotes the decoding order of user k in region i on sub-carrier s for $s \in \mathcal{S}, i \in \mathcal{I}, k \in \mathcal{K}$, where $\psi_{s,i}(k) \in \{0,1\}$ and $\psi_{s,t}(k) + \psi_{s,r}(k) = 1$. For instance, if $\psi_{s,t}(k) = 1$ and $\psi_{s,r}(k) = 0$, it means that user k in region t decodes its signal directly by treating the paired user's signal as interference. Furthermore, user k in region r is capable of using SIC to remove the co-channel interference from the paired user's signal before decoding its own signal. Therefore, the decoding order of SIC in the STAR-RIS-NOMA network considered can be represented as

$$\begin{aligned}\rho_{s,i',k}|\mathbf{h}_{u,s,i,k}^H\mathbf{\Theta}_i\mathbf{G}_s\mathbf{w}_s|^2 &\le \rho_{s,i,k}|\mathbf{h}_{u,s,i,k}^H\mathbf{\Theta}_i\mathbf{G}_s\mathbf{w}_s|^2,\\ \rho_{s,i',k}|\mathbf{h}_{u,s,i',k}^H\mathbf{\Theta}_{i'}\mathbf{G}_s\mathbf{w}_s|^2 &\le \rho_{s,i,k}|\mathbf{h}_{u,s,i',k}^H\mathbf{\Theta}_{i'}\mathbf{G}_s\mathbf{w}_s|^2,\end{aligned} \tag{4}$$

where $i \neq i', i, i' \in \mathcal{I}$, $\psi_{s,i}(k) = 1$ and $\psi_{s,i'}(k) = 0$.

For the considered STAR-RIS-NOMA networks, SIC is exploited at the user with the stronger channel to decode the co-channel interference from the paired user's signal before decoding its own signal. Therefore, based on (4), the signal-to-interference-plus-noise ratio (SINR) of decoding the co-channel interference at the user with the stronger channel is given by

$$r_{u,s,i,k}^{u,s,i,k} = \frac{\rho_{s,i,k}|\mathbf{h}_{u,s,i',k}^H\mathbf{\Theta}_{i'}\mathbf{G}_s\mathbf{w}_s|^2}{\rho_{s,i',k}|\mathbf{h}_{u,s,i',k}^H\mathbf{\Theta}_{i'}\mathbf{G}_s\mathbf{w}_s|^2 + \sigma^2}. \tag{5}$$

The data rate is $R_{u,s,i',k}^{u,s,i,k} = \log_2\left(1 + r_{u,s,i',k}^{u,s,i,k}\right)$. Moreover, in order to guarantee the SIC performed successfully, that is the condition of $R_{u,s,i',k}^{u,s,i,k} \ge R_{u,s,i,k}^{min}$ needs to be satisfied, where $R_{u,s,i,k}^{min}$ denotes the target rate for user k in region i on sub-carrier s.

According to (4), after applying the SIC decoding procedure, the received SINR of the desired signal at the legitimate users on sub-carrier s can be expressed as

$$\begin{aligned}r_{u,s,i,k}^{u,s,i,k} &= \frac{\rho_{s,i,k}|\mathbf{h}_{u,s,i,k}^H\mathbf{\Theta}_i\mathbf{G}_s\mathbf{w}_s|^2}{\rho_{s,i',k}|\mathbf{h}_{u,s,i,k}^H\mathbf{\Theta}_i\mathbf{G}_s\mathbf{w}_s|^2 + \sigma^2},\\ r_{u,s,i',k}^{u,s,i',k} &= \frac{\rho_{s,i',k}|\mathbf{h}_{u,s,i',k}^H\mathbf{\Theta}_{i'}\mathbf{G}_s\mathbf{w}_s|^2}{\sigma^2}.\end{aligned} \tag{6}$$

The data rate are $R_{u,s,i,k}^{u,s,i,k} = \log_2\left(1 + r_{u,s,i,k}^{u,s,i,k}\right)$ and $R_{u,s,i',k}^{u,s,i',k} = \log_2\left(1 + r_{u,s,i',k}^{u,s,i',k}\right)$.

To avoid the secrecy performance loss caused by the uncertainty of the decoding order at the PE, we consider the worst-case assumption, i.e., the PE decodes the signal without suffering from the interference from the same sub-carrier [32]. Therefore, the received SINR of legitimate users at the PE in region i can be expressed as

$$r_{e,s,i,k} = \frac{\rho_{s,i,k}|\mathbf{h}_{e,i}^H\mathbf{\Theta}_i\mathbf{G}_s\mathbf{w}_s|^2}{\sigma^2}, \tag{7}$$

where the date rate of the PE is $R_{e,s,i,k} = \log_2(1 + r_{e,s,i,k})$.

Since the full eavesdropping CSI is available, the channel capacity of the wiretap channels can be evaluated, and thus the secrecy rate is considered as the security metric [33]. The secrecy rate for user k in region i on sub-carrier s is given by

$$R_{s,i,k}^{sec} = [R_{u,s,i,k}^{u,s,i,k} - R_{e,s,i,k}]^+, \tag{8}$$

where $[x]^+ \triangleq \max(x, 0)$. Furthermore, for the statistical eavesdropping CSI, the instantaneous CSI of the PE's channel is not available at the BS. Therefore, we cannot directly evaluate the channel capacity of the wiretap channels. Under this condition, the SOP is an effective security metric used to evaluate the information security performance [37]. Specifically, the positive difference between the codeword rate $R_{u,s,i,k}^{u,s,i,k}$ and the target secrecy rate $\widetilde{R}_{s,i,k}^{sec}$ is the redundant rate to provide security against the PE, and the SOP of user k in region i on sub-carrier s is defined as the probability that the PE's rate $R_{e,s,i,k}$ exceeds the redundant rate. To guarantee the secure transmission of the legitimate users, we consider the worst-case assumption, where the instantaneous rate of the legitimate users are equal to the requirements of QoS [32]. Therefore, the SOP of user k in region i on sub-carrier s is given by

$$P_{s,i,k}^{SOP} = \mathbb{P}(R_{u,s,i,k}^{min} - \widetilde{R}_{s,i,k}^{sec} < R_{e,s,i,k}). \tag{9}$$

To simplify the analysis, we assume that all the receivers undergo a relatively rich scattering environment [38], i.e., all channel fading models degenerate into Rayleigh fading.

B. Problem Formulation for Full Eavesdropping CSI

For full eavesdropping CSI, we aim to maximize the SSR of STAR-RIS-NOMA networks by jointly optimizing the transmission and reflection beamforming of the STAR-RIS, the transmit beamforming of the BS, the power allocation coefficients, and the user pairing vector, subject to the constraints the QoS requirements of each legitimate user, the success of SIC at the receiver side, the total transmit power at the BS, and the SIC decoding order. The optimization problem can be formulated as follows:

$$\max_{\mathbf{\Theta}_i, \mathbf{w}_s, \boldsymbol{\rho}, \boldsymbol{\lambda}} \quad \sum_{s=1}^{S}\sum_{i\in\mathcal{I}}\sum_{k=1}^{K}\lambda_{s,i,k}R_{s,i,k}^{sec} \tag{10a}$$

$$\text{s.t.} \quad R_{u,s,i,k}^{u,s,i,k} \ge R_{u,s,i,k}^{min}, \quad R_{u,s,i',k}^{u,s,i',k} \ge R_{u,s,i',k}^{min}, \tag{10b}$$

$$R_{u,s,i',k}^{u,s,i,k} \ge R_{u,s,i,k}^{min}, \tag{10c}$$

$$\beta_t^m + \beta_r^m = 1, \beta_i^m \in [0,1], \phi_i^m \in [0, 2\pi), \tag{10d}$$

$$\rho_{s,t,k} + \rho_{s,r,k} = 1, \rho_{s,i,k} \in [0,1], \tag{10e}$$

$$\sum_{k=1}^{K}\lambda_{s,i,k} = 1, \lambda_{s,i,k} \in \{0,1\}, \tag{10f}$$

$$\sum_{s=1}^{S}\|\mathbf{w}_s\|^2 \le P_{max}, \tag{10g}$$

$$(4) \quad \& \quad s \in \mathcal{S}, i \neq i', i, i' \in \mathcal{I}, k \in \mathcal{K}, m \in \mathcal{M}, \tag{10h}$$

where P_{max} denotes the constraint on the total transmit power at the BS. Constraint (10b) guarantees the QoS requirement of each legitimate user. Constraint (10c) ensures the success of the SIC decoding. Constraint (10d) represents the amplitude and phase shift requirements for each element of the STAR-RIS. Constraint (10e) indicates the power allcoation of

each sub-carrier. Constraint (10f) guarantees the paired users in each sub-carrier come from different regions. Constraint (10g) limits the total transmit power at the BS. Constraint (10h) determines the SIC decoding order of the legitimate users.

C. Problem Formulation for Statistical Eavesdropping CSI

For statistical eavesdropping CSI, the joint optimization maximum SOP minimization problem of the transmission and reflection beamforming of the STAR-RIS, the transmit beamforming of the BS, the power allocation coefficients, and the user pairing vector can be formulated as follows:

$$\min_{\boldsymbol{\Theta}_i, \mathbf{w}_s, \boldsymbol{\rho}, \boldsymbol{\lambda}} \quad \max_{s\in\mathcal{S}, i\in\mathcal{I}, k\in\mathcal{K}} \lambda_{s,i,k} P_{s,i,k}^{SOP} \tag{11a}$$

$$\text{s.t.} \quad (10b) - (10h). \tag{11b}$$

The main challenges of solving the optimization problems formulated in (10) and (11) can be summarized as follows. Firstly, the user pairing problem is a mixed-integer problem, which is non-convex. Secondly, STAR-RIS requires the optimization of two types of passive beamforming, i.e., transmission and reflection passive beamforming, which complicates the optimization of the SIC decoding order. Finally, due to the coupled optimization variables as well as the non-convex objective function and constraints, the formulated optimization problem (10) and (11) are intricate for obtaining the optimal solution.

IV. Approximation Solution for the Full Eavesdropping CSI Scheme

In this section, we propose an alternating beamforming algorithm for maximizing the SSR of the multi-carrier STAR-RIS-NOMA network by decomposing the original problem into three subproblems, where the beamforming vectors are obtained by alternately solving the user pairing subproblem and the joint beamforming optimization subproblem. With the obtained beamforming vectors, the power allcoation subproblem is solved by an iterative algorithm.

A. User Pairing

In this subsection, we first optimize the user pairing vector $\boldsymbol{\lambda}$. Giving a set of feasible $\{\boldsymbol{\Theta}_i, \mathbf{w}_s, \boldsymbol{\rho}\}$, the subproblem of optimizing the user pairing can be formulated as follows:

$$\max_{\boldsymbol{\lambda}} \quad \sum_{s=1}^{S}\sum_{i\in\mathcal{I}}\sum_{k=1}^{K} \lambda_{s,i,k} R_{s,i,k}^{sec} \tag{12a}$$

$$\text{s.t.} \quad (10f), \tag{12b}$$

which is a combinatorial optimization problem. To tackle this problem, one traditional method is to search all the user pairing combinations. However, the computational complexity grows significantly as the number of the granted users increase [17]. Therefore, we develop a KM algorithm based on the differences of users' channel gains for achieving a tade-off between complexity and performance. The core idea of the KM algorithm is to maximize the difference of the channel gains between the paired users.

To perform the KM algorithm, we introduce some basic definitions.

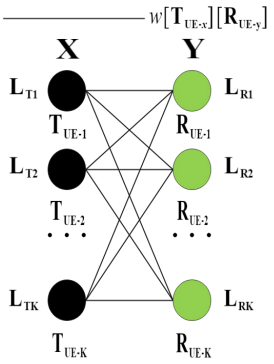

Fig. 2. The UE pairing model between T region and R region.

Algorithm 1 KM Algorithm for User Pairing

Initialization:
Initialize the transmission and reflection coefficient vectors $\mathbf{v}_i^*$ according to (14). Then, all users evaluate their equivalent channel gains $\|\mathbf{v}_i^H \mathbf{H}_{u,s,i,k}\|^2$.
Compute the weight value between all users in X and Y according to the difference of the channel gain.
Set the label of each user according to (15) and $n = 1$.

repeat
  User $\mathrm{T}_{\text{UE-}n}$ in X selects user $\mathrm{R}_{\text{UE-}k}$ in Y to perform paired based on the matching principle of maximizing the channel gain difference.
  if The matching of the user $\mathrm{T}_{\text{UE-}n}$ does not conflict with other users in X **then**
    User $\mathrm{T}_{\text{UE-}n}$ is paired.
  else
    Compute $d = \min\{L_{Tn} + L_{Rk'} - w[\mathrm{T}_{\text{UE-}n}][\mathrm{R}_{\text{UE-}k'}], L_{Tn'} + L_{Rk'} - w[\mathrm{T}_{\text{UE-}n'}][\mathrm{R}_{\text{UE-}k'}]\}, n' \in \mathcal{K}\backslash\{n\}, k' \in \mathcal{K}\backslash\{k\}$, where user $\mathrm{T}_{\text{UE-}n'}$ is in conflict with user $\mathrm{T}_{\text{UE-}n}$.
    Based on the label adjustment value d, user $\mathrm{T}_{\text{UE-}n}$ and user $\mathrm{T}_{\text{UE-}n'}$ in X decrease the label and user $\mathrm{R}_{\text{UE-}k}$ in Y increases the label.
    Update user pairing based on the condition of $L_{Tx} + L_{Ry} = w[\mathrm{T}_{\text{UE-}x}][\mathrm{R}_{\text{UE-}y}], x \in \mathcal{K}, y \in \mathcal{K}$.
  end if
  $n = n + 1$.
until All of the users are paired.

1) Channel Gain: Let $\mathbf{v}_i = [\sqrt{\beta_i^1} e^{j\phi_i^1}, ..., \sqrt{\beta_i^M} e^{j\phi_i^M}]^H, i \in \mathcal{I}$, the channel gain of user k in region i on sub-carrier s can be rewritten as follows:

$$\|\mathbf{h}_{u,s,i,k}^H \boldsymbol{\Theta}_i \mathbf{G}_s\|^2 = \|\mathbf{v}_i^H \mathbf{H}_{u,s,i,k}\|^2, \tag{13}$$

where $\mathbf{H}_{u,s,i,k} = \mathrm{diag}(\mathbf{h}_{u,s,i,k}^H)\mathbf{G}_s$. Note that the channel gain in (13) relys on the variables $\mathbf{v}_i$. We can initialize the transmission and reflection coefficient vectors as [17]

$$\beta_i^m = 0.5, \phi_i^m = -\mathrm{angle}(\upsilon_i^*), i \in \mathcal{I}, m \in \mathcal{M}, \tag{14}$$

where υ_i^* is the element of the optimal transmission or reflection coefficient vectors $\mathbf{v}_i^*$. It can calculated as $\mathbf{v}_i^* = \arg\max_{\mathbf{v}_i} \|\mathbf{v}_i^H \mathbf{H}_{u,s,i,k}\|^2, i \in \mathcal{I}$.

2) Set, Label and Weight Value: As shown in Fig. 2, we define the user sets of the T and R regions as X and Y, respectively, denoted by $X \triangleq \mathcal{T}$ and $Y \triangleq \mathcal{R}$. Then, we define the user labels in X and Y as $\{L_{T1}, ..., L_{TK}\}$ and $\{L_{R1}, ..., L_{RK}\}$, respectively. Furthermore, the difference of the channel gain is used to define the value of the weight between users in X and Y, denoted by $w[\mathrm{T_{UE}}\text{-}x][\mathrm{R_{UE}}\text{-}y]$, $x \in \mathcal{K}$, $y \in \mathcal{K}$.

Firstly, based on (13) and (14), we initialize all users' channel gains. Then, based on the greedy selection method, the labels in X can be evaluated as follows:

$$L_{Tk} = \max\{w[\mathrm{T_{UE}}\text{-}k][\mathrm{R_{UE}}\text{-}y]\}, x \in \mathcal{K}, \forall y \in \mathcal{K}. \tag{15}$$

Furthermore, all labels in Y are 0. Secondly, based on the matching principle of maximizing the difference of the channel gain between the users in X and Y, user $\mathrm{T_{UE}}\text{-}n$ in X selects user $\mathrm{R_{UE}}\text{-}k$ in Y with the largest difference of the channel gain to be paired. If the matching of the user $\mathrm{T_{UE}}\text{-}n$ does not conflict with other users in X, the user $\mathrm{T_{UE}}\text{-}n$ successfully pairs with user $\mathrm{R_{UE}}\text{-}k$ in Y. If user $\mathrm{T_{UE}}\text{-}n'$ has paired with user $\mathrm{R_{UE}}\text{-}k$, which is matching conflict with user $\mathrm{T_{UE}}\text{-}n$. To overcome this difficulty, we consider to adjust the labels of all users (i.e., $\mathrm{T_{UE}}\text{-}n$, $\mathrm{T_{UE}}\text{-}n'$ and $\mathrm{R_{UE}}\text{-}k$) that are in conflict. Specifically, user $\mathrm{T_{UE}}\text{-}n$ and user $\mathrm{T_{UE}}\text{-}n'$ in X decrease the label and user $\mathrm{R_{UE}}\text{-}k$ in Y increases the label. The amount of label adjustment is defined as $d = \min\{L_{Tn} + L_{Rk'} - w[\mathrm{T_{UE}}\text{-}n][\mathrm{R_{UE}}\text{-}k'], L_{Tn'} + L_{Rk'} - w[\mathrm{T_{UE}}\text{-}n'][\mathrm{R_{UE}}\text{-}k']\}, n' \in \mathcal{K}\backslash\{n\}, k' \in \mathcal{K}\backslash\{k\}$. After updating the label, the user pairing scheme is determined according to the condition $L_{Tx} + L_{Ry} = w[\mathrm{T_{UE}}\text{-}x][\mathrm{R_{UE}}\text{-}y], x \in \mathcal{K}, y \in \mathcal{K}$. Finally, the subsequent users rely on a similar method for matching until all the users are paired.

The details of the proposed KM algorithm are summarized in Algorithm 1. As for the complexity, user selection has the complexity of $\mathcal{O}(K)$, and the maximum complexity of label adjustment for each user selection is $\mathcal{O}(K)$. Furthermore, the complexity of finding d is $\mathcal{O}(K)$. Therefore, the computational complexity of the KM algorithm is given by $\mathcal{O}(K^3)$.

B. Joint Beamforming Optimization

In this subsection, we propose an iterative algorithm for jointly optimizing the transmission and reflection beamforming of STAR-RIS, and the transmit beamforming of the BS.

Based on the user pairing described in Section IV-A, we omit the index k for simplicity. Consider $\mathbf{H}_{u,s,i} = \mathrm{diag}(\mathbf{h}_{u,s,i}^H)\mathbf{G}_s$ and $\mathbf{H}_{e,i} = \mathrm{diag}(\mathbf{h}_{e,i}^H)\mathbf{G}_s, s \in \mathcal{S}, i \in \mathcal{I}$. Moreover, we define $\mathbf{V}_i = \mathbf{v}_i\mathbf{v}_i^H, \forall i \in \mathcal{I}$, with $\mathbf{V}_i \succeq 0$ and $\mathrm{Rank}(\mathbf{V}_i) = 1$. Similarly, we define $\mathbf{W}_s = \mathbf{w}_s\mathbf{w}_s^H, \forall s \in \mathcal{S}$, which satisfies the conditions $\mathbf{W}_s \succeq 0$ and $\mathrm{Rank}(\mathbf{W}_s) = 1$. Note that $\{\mathbf{v}_i^*\}_{i\in\mathcal{I}}$ and $\{\mathbf{w}_s^*\}_{s\in\mathcal{S}}$ can be obtained using decomposition, if $\{\mathbf{V}_i^*\}_{i\in\mathcal{I}}$ and $\{\mathbf{W}_s^*\}_{s\in\mathcal{S}}$ are full rank, otherwise, $\{\mathbf{v}_i^*\}_{i\in\mathcal{I}}$ and $\{\mathbf{w}_s^*\}_{s\in\mathcal{S}}$ can be obtained by Gaussian randomization [39]. Given the power allocation coefficients $\boldsymbol{\rho}$, the subproblem of joint beamforming optimization can be expressed as:

$$\max_{\mathbf{V}_t,\mathbf{V}_r,\mathbf{W}_s} \quad \sum_{s=1}^{S}\sum_{i\in\mathcal{I}} R_{s,i}^{sec} \tag{16a}$$

$$\text{s.t.} \quad \frac{\rho_{s,i}\mathrm{Tr}(\mathbf{H}_{u,s,i}\mathbf{W}_s\mathbf{H}_{u,s,i}^H\mathbf{V}_i)}{\rho_{s,i'}\mathrm{Tr}(\mathbf{H}_{u,s,i}\mathbf{W}_s\mathbf{H}_{u,s,i}^H\mathbf{V}_i)+\sigma^2} \geq \gamma_{u,s,i}, \tag{16b}$$

$$\frac{\rho_{s,i}\mathrm{Tr}(\mathbf{H}_{u,s,i'}\mathbf{W}_s\mathbf{H}_{u,s,i'}^H\mathbf{V}_{i'})}{\rho_{s,i'}\mathrm{Tr}(\mathbf{H}_{u,s,i'}\mathbf{W}_s\mathbf{H}_{u,s,i'}^H\mathbf{V}_{i'})+\sigma^2} \geq \gamma_{u,s,i}, \tag{16c}$$

$$\rho_{s,i'}\mathrm{Tr}(\mathbf{H}_{u,s,i}\mathbf{W}_s\mathbf{H}_{u,s,i}^H\mathbf{V}_i) \leq \rho_{s,i}\mathrm{Tr}(\mathbf{H}_{u,s,i}\mathbf{W}_s\mathbf{H}_{u,s,i}^H\mathbf{V}_i),$$
$$\rho_{s,i'}\mathrm{Tr}(\mathbf{H}_{u,s,i'}\mathbf{W}_s\mathbf{H}_{u,s,i'}^H\mathbf{V}_{i'}) \leq \rho_{s,i}\mathrm{Tr}(\mathbf{H}_{u,s,i'}\mathbf{W}_s\mathbf{H}_{u,s,i'}^H\mathbf{V}_{i'}), \tag{16d}$$

$$\mathbf{V}_t(m,m) + \mathbf{V}_r(m,m) = 1, \tag{16e}$$

$$\sum_{s=1}^{S}\mathrm{Tr}(\mathbf{W}_s) \leq P_{max}, \tag{16f}$$

$$\mathbf{V}_t \succeq 0, \mathbf{V}_r \succeq 0, \mathbf{W}_s \succeq 0, \tag{16g}$$

$$s \in \mathcal{S}, i \neq i', i, i' \in \mathcal{I}, m \in \mathcal{M}, \tag{16h}$$

where $\gamma_{u,s,i}$ is the received SINR threshold for the user in region i on sub-carrier s. Problem (16) is non-convex due to the highly-coupled non-convex terms in (16a), (16b), (16c) and (16d).

To tackle this challenging problem, we firstly evaluate an upper bound $\bar{L}_{u,s,i}$ and a lower bound $\underline{L}_{u,s,i}$ of $\mathrm{Tr}(\mathbf{H}_{u,s,i}\mathbf{W}_s\mathbf{H}_{u,s,i}^H\mathbf{V}_i)$ in (16), respectively. According to [34], i.e., $\mathrm{Tr}(\mathbf{AB}) = \frac{1}{2}\|\mathbf{A}+\mathbf{B}\|_F^2 - \frac{1}{2}\|\mathbf{A}\|_F^2 - \frac{1}{2}\|\mathbf{B}\|_F^2$, where $\mathbf{A}$ and $\mathbf{B}$ denote Hermitian matrices with the same size, the upper bound $\bar{L}_{u,s,i}$, and the lower bound $\underline{L}_{u,s,i}$ can be given as follows:

$$2\bar{L}_{u,s,i} \geq 2\mathrm{Tr}(\mathbf{H}_{u,s,i}\mathbf{W}_s\mathbf{H}_{u,s,i}^H\mathbf{V}_i) = \|\mathbf{H}_{u,s,i}\mathbf{W}_s\mathbf{H}_{u,s,i}^H + \mathbf{V}_i\|_F^2 \underbrace{-\|\mathbf{H}_{u,s,i}\mathbf{W}_s\mathbf{H}_{u,s,i}^H\|_F^2 - \|\mathbf{V}_i\|_F^2}_{\Xi}, \tag{17}$$

and

$$2\mathrm{Tr}(\mathbf{H}_{u,s,i}\mathbf{W}_s\mathbf{H}_{u,s,i}^H\mathbf{V}_i) = \underbrace{\|\mathbf{H}_{u,s,i}\mathbf{W}_s\mathbf{H}_{u,s,i}^H + \mathbf{V}_i\|_F^2}_{\Psi} - \|\mathbf{H}_{u,s,i}\mathbf{W}_s\mathbf{H}_{u,s,i}^H\|_F^2 - \|\mathbf{V}_i\|_F^2 \geq 2\underline{L}_{u,s,i}. \tag{18}$$

To guarantee the equivalent transformations in (17) and (18), we should ensure that (17) and (18) are convex. By leveraging the first-order Taylor expansion of Ξ and Ψ, the upper bound $\bar{L}_{u,s,i}$ and the lower bound $\underline{L}_{u,s,i}$ can be rewritten as

$$2\bar{L}_{u,s,i} \geq \|\mathbf{H}_{u,s,i}\mathbf{W}_s\mathbf{H}_{u,s,i}^H + \mathbf{V}_i\|_F^2 + \|\mathbf{H}_{u,s,i}\widetilde{\mathbf{W}}_s^{(n)}\mathbf{H}_{u,s,i}^H\|_F^2 - 2\mathrm{Tr}\Big((\mathbf{H}_{u,s,i}\widetilde{\mathbf{W}}_s^{(n)}\mathbf{H}_{u,s,i}^H)^H(\mathbf{H}_{u,s,i}\mathbf{W}_s\mathbf{H}_{u,s,i}^H)\Big) + \|\widetilde{\mathbf{V}}_i^{(n)}\|_F^2 - 2\mathrm{Tr}\Big((\widetilde{\mathbf{V}}_i^{(n)})^H\mathbf{V}_i\Big), \tag{19}$$

and

$$2\mathrm{Tr}\Big((\mathbf{H}_{u,s,i}\widetilde{\mathbf{W}}_s^{(n)}\mathbf{H}_{u,s,i}^H + \widetilde{\mathbf{V}}_i^{(n)})^H(\mathbf{H}_{u,s,i}\mathbf{W}_s\mathbf{H}_{u,s,i}^H + \mathbf{V}_i)\Big) - \|\mathbf{H}_{u,s,i}\widetilde{\mathbf{W}}_s^{(n)}\mathbf{H}_{u,s,i}^H + \widetilde{\mathbf{V}}_i^{(n)}\|_F^2 - \|\mathbf{H}_{u,s,i}\mathbf{W}_s\mathbf{H}_{u,s,i}^H\|_F^2 - \|\mathbf{V}_i\|_F^2 \geq 2\underline{L}_{u,s,i}, \tag{20}$$

where $\widetilde{\mathbf{W}}_s^{(n)}$ and $\widetilde{\mathbf{V}}_i^{(n)}$ denote the value of the variable $\mathbf{W}_s$ and $\mathbf{V}_i$ at the nth iteration, respectively. Therefore, based on (19) and (20), the constraint (16b) can be transformed into a convex form, which is given by

$$\rho_{s,i}\underline{L}_{u,s,i} \geq \rho_{s,i'}\bar{L}_{u,s,i}\gamma_{u,s,i} + \sigma^2\gamma_{u,s,i},$$

$$\rho_{s,i'}\underline{L}_{u,s,i'} \geq \sigma^2\gamma_{u,s,i'}. \tag{21}$$

Similarly, the constraints (16c) and (16d) can be transformed into the convex forms

$$\rho_{s,i}\underline{L}_{u,s,i'} \geq \rho_{s,i'}\bar{L}_{u,s,i'}\gamma_{u,s,i} + \sigma^2\gamma_{u,s,i} \tag{22}$$

and

$$\rho_{s,i'}\bar{L}_{u,s,i} \leq \rho_{s,i}\underline{L}_{u,s,i}, \rho_{s,i'}\bar{L}_{u,s,i'} \leq \rho_{s,i}\underline{L}_{u,s,i'}, \tag{23}$$

respectively. Based on (19) and (20), the lower bound of the SSR can be expressed as

$$\sum_{s=1}^{S}\sum_{i\in\mathcal{I}} R_{s,i}^{sec,l} = \sum_{s=1}^{S}\sum_{i\in\mathcal{I}} \log_2\left(\frac{1+r_{u,s,i}^{u,s,i,l}}{1+r_{e,s,i}^{u}}\right), \tag{24}$$

where

$$\begin{aligned}
r_{u,s,i}^{u,s,i} \geq r_{u,s,i}^{u,s,i,l} &= \frac{\rho_{s,i}\underline{L}_{u,s,i}}{\rho_{s,i'}\bar{L}_{u,s,i}+\sigma^2},\\
r_{u,s,i'}^{u,s,i'} \geq r_{u,s,i'}^{u,s,i',l} &= \frac{\rho_{s,i'}\underline{L}_{u,s,i'}}{\sigma^2},\\
r_{e,s,i} \leq r_{e,s,i}^{u} &= \frac{\rho_{s,i}\bar{L}_{e,s,i}}{\sigma^2},\\
r_{e,s,i'} \leq r_{e,s,i'}^{u} &= \frac{\rho_{s,i'}\bar{L}_{e,s,i'}}{\sigma^2}.
\end{aligned} \tag{25}$$

Here, $\bar{L}_{e,s,i}$ denotes the upper bound of $\mathrm{Tr}(\mathbf{H}_{e,i}\mathbf{W}_s\mathbf{H}_{e,i}^H\mathbf{V}_i)$ in (16a). Similar to (19) and (20), the upper bound of $\mathrm{Tr}(\mathbf{H}_{e,i}\mathbf{W}_s\mathbf{H}_{e,i}^H\mathbf{V}_i)$ is given by

$$\begin{aligned}
2\bar{L}_{e,s,i} \geq\ & \|\mathbf{H}_{e,i}\mathbf{W}_s\mathbf{H}_{e,i}^H + \mathbf{V}_i\|_F^2 + \|\mathbf{H}_{e,i}\widetilde{\mathbf{W}}_s^{(n)}\mathbf{H}_{e,i}^H\|_F^2\\
&- 2\mathrm{Tr}\Big((\mathbf{H}_{e,i}\widetilde{\mathbf{W}}_s^{(n)}\mathbf{H}_{e,i}^H)^H(\mathbf{H}_{e,i}\mathbf{W}_s\mathbf{H}_{e,i}^H)\Big) + \|\widetilde{\mathbf{V}}_i^{(n)}\|_F^2\\
&- 2\mathrm{Tr}\Big((\widetilde{\mathbf{V}}_i^{(n)})^H\mathbf{V}_i\Big).
\end{aligned} \tag{26}$$

Note that the objective function in (24) is still challenging due to the coupled variables. To handle this issue, we evaluate the lower bound $\underline{U}_{u,s,i}$ of the SINR for the legitimate users $r_{u,s,i}^{u,s,i,l}$ in (25) and the upper bound $\bar{U}_{e,s,i}$ of the SINR for the PEs $r_{e,s,i}^{u}$ in (25), respectively, which are given by

$$\begin{aligned}
\rho_{s,i}\underline{L}_{u,s,i} &\geq (\rho_{s,i'}\bar{L}_{u,s,i}+\sigma^2)\underline{U}_{u,s,i},\\
\rho_{s,i'}\underline{L}_{u,s,i'} &\geq \sigma^2\underline{U}_{u,s,i'},\\
\rho_{s,i}\bar{L}_{e,s,i} &\leq \sigma^2\bar{U}_{e,s,i},\\
\rho_{s,i'}\bar{L}_{e,s,i'} &\leq \sigma^2\bar{U}_{e,s,i'}.
\end{aligned} \tag{27}$$

According to the inequality, i.e., $2xy \leq (ex)^2 + (\frac{y}{e})^2$, where the equality holds if and only if $e = \sqrt{\frac{y}{x}}$ and x, y are any non-negative variables, the lower bound $\underline{U}_{u,s,i}$ and the upper bound $\bar{U}_{e,s,i}$ in (27) can be rewritten as

$$\begin{aligned}
\rho_{s,i}\underline{L}_{u,s,i} &\geq \frac{1}{2}\left(e_{s,i}^{(n)2}(\rho_{s,i'}\bar{L}_{u,s,i}+\sigma^2)^2 + \frac{(\underline{U}_{u,s,i})^2}{e_{s,i}^{(n)2}}\right),\\
\rho_{s,i'}\underline{L}_{u,s,i'} &\geq \sigma^2\underline{U}_{u,s,i'},\\
\rho_{s,i}\bar{L}_{e,s,i} &\leq \sigma^2\bar{U}_{e,s,i},\\
\rho_{s,i'}\bar{L}_{e,s,i'} &\leq \sigma^2\bar{U}_{e,s,i'},
\end{aligned} \tag{28}$$

Algorithm 2 Proposed SCA Based Iterative Algorithm for Solving Problem (16)

1: **Initialization:**
Initialize the iteration parameters $\zeta^{(0)} = 0$, $e_{s,i}^{(0)} = 0$, $t_{s,i}^{(0)} = 0$, $\widetilde{\mathbf{V}}_i^{(0)} = \mathbf{I}_M$, $\widetilde{\mathbf{W}}_s^{(0)} = \mathbf{I}_N$, the power allocation coefficient $\rho_{s,i} = 0.5$, $n = 1$, $\Delta_1 = 1$ and the convergence tolerance $\epsilon_1 = 10^{-4}$.
Initialize the user pairing vector $\boldsymbol{\lambda}$ and the SIC decoding order $\psi_{s,i}$ via **Algorithm 1**.
2: **while** $\Delta_1 \geq \epsilon_1$ **do**
3: Update $\zeta^{(n)}$, $\mathbf{V}_i^{(n-1)}$, $\mathbf{W}_s^{(n-1)}$, $\bar{L}_{u,s,i}^{(n-1)}$, $\underline{U}_{u,s,i}^{(n-1)}$ and $\bar{U}_{e,s,i}^{(n-1)}$ by solving problem (30).
4: Update $\widetilde{\mathbf{V}}_i^{(n)} = \mathbf{V}_i^{(n-1)}$, $\widetilde{\mathbf{W}}_s^{(n)} = \mathbf{W}_s^{(n-1)}$, $t_{s,i}^{(n)} = \log_2\left(\frac{1+\underline{U}_{u,s,i}^{(n-1)}}{1+\bar{U}_{e,s,i}^{(n-1)}}\right)$, $e_{s,i}^{(n)} = \sqrt{\frac{\underline{U}_{u,s,i}^{(n-1)}}{\rho_{s,i'}\bar{L}_{u,s,i}^{(n-1)}+\sigma^2}}$.
5: Update $\Delta_1 = |\zeta^{(n)} - \zeta^{(n-1)}|$.
6: $n = n+1$.
7: **end while**

where $e_{s,i}^{(n)} = \sqrt{\frac{\underline{U}_{u,s,i}^{(n-1)}}{\rho_{s,i'}\bar{L}_{u,s,i}^{(n-1)}+\sigma^2}}$ represents the value of $e_{s,i}$ at the nth iteration. As a result, by using the epigraph reformulation [31], the problem (16) can be transformed into an approximated problem as follows:

$$\max_{\substack{\mathbf{V}_t,\mathbf{V}_r,\mathbf{W}_s,\bar{L}_{u,s,i},\underline{L}_{u,s,i},\bar{L}_{e,s,i},\\ \underline{U}_{u,s,i},\bar{U}_{e,s,i},\boldsymbol{t},\tau}} \quad \tau \tag{29a}$$

$$\text{s.t.} \quad \tau = \sum_{s=1}^{S}\sum_{i\in\mathcal{I}} t_{s,i}, \tag{29b}$$

$$\log_2\left(\frac{1+\underline{U}_{u,s,i}}{1+\bar{U}_{e,s,i}}\right) \geq t_{s,i}, \tag{29c}$$

$$(16e)-(16h), (19)-(23), (26), (28), \tag{29d}$$

where τ and $\boldsymbol{t} = \{t_{1,t}, t_{1,r}, ..., t_{S,r}\}$ are an auxiliary non-negative optimization variable and non-negative optimization variable vector, respectively. Note that the problem (29) remains non-convex, since the constraint (29c) is non-convex. To overcome this issue, we transform the vector $\boldsymbol{t}$ into the iteration coefficients. Therefore, the problem (29) can be further transformed as follows:

$$\max_{\substack{\mathbf{V}_t,\mathbf{V}_r,\mathbf{W}_s,\bar{L}_{u,s,i},\underline{L}_{u,s,i},\bar{L}_{e,s,i},\\ \underline{U}_{u,s,i},\bar{U}_{e,s,i},\boldsymbol{\xi},\zeta}} \quad \zeta \tag{30a}$$

$$\text{s.t.} \quad \zeta = \sum_{s=1}^{S}\sum_{i\in\mathcal{I}} \xi_{s,i}, \tag{30b}$$

$$1+\underline{U}_{u,s,i} - 2^{t_{s,i}}(1+\bar{U}_{e,s,i}) \geq \xi_{s,i}, \tag{30c}$$

$$(16e)-(16h), (19)-(23), (26), (28), \tag{30d}$$

where ζ is an auxiliary non-negative optimization variable, $t_{s,i} = \log_2\left(\frac{1+\underline{U}_{u,s,i}^{(n-1)}}{1+\bar{U}_{e,s,i}^{(n-1)}}\right)$ in the nth iteration, $\boldsymbol{\xi} = \{\xi_{1,t}, \xi_{1,r}, ..., \xi_{S,r}\}$ is an auxiliary non-negative optimization variable vector, which is introduced to measure the

Algorithm 3 Power Allocation Coefficients Optimization Algorithm

Initialization:
Initialize the iteration parameters $q^{(0)}=0$, $a_{u,s,i}^{(0)}=0$, $a_{e,s,i}^{(0)}=0$, $n=1$, $\Delta_2=1$ and the convergence tolerance $\epsilon_2=10^{-4}$.
Initialize the user pairing vector $\boldsymbol{\lambda}$ and the SIC decoding order $\psi_{s,i}$ via **Algorithm 1**.
Initialize the passive and transmit beamforming $\mathbf{V}_i$, $\mathbf{W}_s$ via **Algorithm 2**.
while $\Delta_2 \geq \epsilon_2$ **do**
  Update $q^{(n)}$, $\rho_{s,i}^{(n-1)}$ by solving problem (33).
  Update $a_{u,s,t}^{(n)}=\frac{1}{\rho_{s,r}^{(n-1)}\Lambda_{u,s,t}+\sigma^2}$, if $\psi_{s,t}=1$, $\psi_{s,r}=0$ or $a_{u,s,r}^{(n)}=\frac{1}{\rho_{s,t}^{(n-1)}\Lambda_{u,s,r}+\sigma^2}$, if $\psi_{s,r}=1$, $\psi_{s,t}=0$, $a_{e,s,i}^{(n)}=\frac{1}{\rho_{s,i}^{(n-1)}\Lambda_{e,s,i}+\sigma^2}$.
  Update $\Delta_2=|q^{(n)}-q^{(n-1)}|$.
  $n=n+1$.
end while

approximation gap between $\log_2\left(\frac{1+\underline{U}_{u,s,i}}{1+\bar{U}_{e,s,i}}\right)$ and $t_{s,i}$. Now, the problem (30) is a standard convex problem, which can be effectively solved by using the existing toolboxes, such as CVX [40].

The details of the proposed SCA based algorithm are summarized in Algorithm 2. First, the iterative process begins by initializing the iteration parameters $\{\zeta^{(0)}, e_{s,i}^{(0)}, t_{s,i}^{(0)}, \widetilde{\mathbf{V}}_i^{(0)}, \widetilde{\mathbf{W}}_s^{(0)}\}$ and the power allocation coefficient $\rho_{s,i}$. In the algorithm, $\{\mathbf{V}_i, \mathbf{W}_s\}$ are jointly optimized by iteratively solving the problem (30). Specifically, $\{\zeta^{(n)}, \mathbf{V}_i^{(n-1)}, \mathbf{W}_s^{(n-1)}, \bar{L}_{u,s,i}^{(n-1)}, \underline{U}_{u,s,i}^{(n-1)}, \bar{U}_{e,s,i}^{(n-1)}\}$ can be obtained by solving problem (30). Then, the values of $\{\widetilde{\mathbf{V}}_i^{(n)}, \widetilde{\mathbf{W}}_s^{(n)}, t_{s,i}^{(n)}, e_{s,i}^{(n)}\}$ can be updated after each iteration. If the gap between the successive iterations of the object function is less than the threshold ϵ_1, the iterative procedure will stop. Note that the SSR is increasing in each iteration, and an upper bound of SSR exists due to the total transmit power constraint of the BS. Therefore, the convergence of Algorithm 2 is guaranteed.

The computational complexity of Algorithm 2 is mainly dominated by solving the problem (30). Therefore, the complexity of Algorithm 2 for solving problem (16) is $\mathcal{O}\Big((6K+3)(M+1)^{\frac{7}{2}}+(6K+1+S)^3(N+1)^{\frac{1}{2}}\Big)L_1\log(\epsilon_1^{-1})$, where L_1 is the number of iterations of Algorithm 2.

C. Power Allocation Optimization

Given $\{\mathbf{V}_i\}_{i\in\mathcal{I}}$ and $\{\mathbf{W}_s\}_{s\in\mathcal{S}}$, the subproblem of power allocation in (10) can be reformulated as:

$$\max_{\boldsymbol{\rho},q} \quad q \tag{31a}$$

$$\text{s.t.} \quad \sum_{s=1}^{S}\sum_{i\in\mathcal{I}} R_{s,i}^{sec} \geq q, \tag{31b}$$

$$\rho_{s,t}+\rho_{s,r}=1, \rho_{s,i}\in[0,1], \tag{31c}$$

$$(16b)-(16d), (16h), \tag{31d}$$

Algorithm 4 Alternating Beamforming Algorithm

Initialization:
Initialize the passive beamforming $\widehat{\mathbf{V}}_i^{(0)}$ according to (14). Set $n=1$.
repeat
  Compute $\boldsymbol{\lambda}^{(n-1)}$ via **Algorithm 1**.
  Compute $\mathbf{V}_i^{(n-1)}$ via **Algorithm 2**.
  Update $\widehat{\mathbf{V}}_i^{(n)}=\mathbf{V}_i^{(n-1)}$.
  $n=n+1$.
until Two consecutive user pairing vectors are the same.
Optimize the power allocation coefficients via **Algorithm 3**.

where $q\geq 0$. Note that the constraint in (31b) is non-convex. Therefore, we focus on handling the constraint (31b) in the following.

For ease of exposition, denote $\Lambda_{u,s,i}=\mathrm{Tr}(\mathbf{H}_{u,s,i}\mathbf{W}_s\mathbf{H}_{u,s,i}^H\mathbf{V}_i)$ and $\Lambda_{e,s,i}=\mathrm{Tr}(\mathbf{H}_{e,i}\mathbf{W}_s\mathbf{H}_{e,i}^H\mathbf{V}_i)$, $\forall s\in\mathcal{S}, \forall i\in\mathcal{I}$. According to SLB approximate [41], i.e., $-\log_2 b\geq -\frac{ab}{\ln 2}+\log_2 a+\frac{1}{\ln 2}$, where a is a positive scalar and the equality holds if and only if $a=\frac{1}{b}$, the constraint (31b) can be rewritten as

$$\begin{aligned}\sum_{s=1}^{S}\Bigg[&\log_2\left(\rho_{s,t}\Lambda_{u,s,t}+\psi_{s,t}\rho_{s,r}\Lambda_{u,s,t}+\sigma^2\right)+2\log_2\left(\sigma^2\right)\\&+\log_2\left(\rho_{s,r}\Lambda_{u,s,r}+\psi_{s,r}\rho_{s,t}\Lambda_{u,s,r}+\sigma^2\right)+\log_2 a_{u,s,t}^{(n)}\\&-\frac{a_{u,s,t}^{(n)}}{\ln 2}\left(\psi_{s,t}\rho_{s,r}\Lambda_{u,s,t}+\sigma^2\right)+\log_2 a_{u,s,r}^{(n)}\\&-\frac{a_{u,s,r}^{(n)}}{\ln 2}\left(\psi_{s,r}\rho_{s,t}\Lambda_{u,s,r}+\sigma^2\right)+\quad\log_2 a_{e,s,t}^{(n)}\\&-\frac{a_{e,s,t}^{(n)}}{\ln 2}\left(\rho_{s,t}\Lambda_{e,s,t}+\sigma^2\right)+\log_2 a_{e,s,r}^{(n)}\\&-\frac{a_{e,s,r}^{(n)}}{\ln 2}\left(\rho_{s,r}\Lambda_{e,s,r}+\sigma^2\right)+\frac{4}{\ln 2}\Bigg]\geq q,\end{aligned} \tag{32}$$

where $a_{u,s,t}^{(n)}$, $a_{u,s,r}^{(n)}$, $a_{e,s,t}^{(n)}$ and $a_{e,s,r}^{(n)}$ represent the values of $a_{u,s,t}$, $a_{u,s,r}$, $a_{e,s,t}$ and $a_{e,s,r}$ at the nth iteration, respectively. The proof of (32) is provided in Appendix. Therefore, the optimization problem in (31) can be transformed into an approximated convex problem as follows:

$$\max_{\boldsymbol{\rho},q} \quad q \tag{33a}$$

$$\text{s.t.} \quad \rho_{s,t}+\rho_{s,r}=1, \rho_{s,i}\in[0,1], \tag{33b}$$

$$(16b)-(16d), (16h), (32), \tag{33c}$$

which can be solved by CVX. Note that the convex problem (33) can be solved by iteratively using the SLB approximation until convergence. Specifically, the variable $q^{(n)}$ can be obtained by solving problem (33) using the SLB approximation until the gap between the successive iterations of the object function is less than the threshold ϵ_2. The process of optimizing the power allocation coefficients is summarized in Algorithm 3.

Note that the convergence of Algorithm 3 is guaranteed, because the SSR increases in each iteration, and an upper

bound for the SSR exists. Moreover, the complexity of Algorithm 3 is $\mathcal{O}\Big((10K+1)^3(2)^{\frac{1}{2}}\Big)L_2\log(\epsilon_2^{-1})$, where L_2 is the number of iterations of Algorithm 3.

D. Overall Algorithm

In order to obtain the beamforming vectors, we develop an alternating beamforming algorithm for beamforming design. Specifically, we first initialize the passive beamforming $\widehat{\mathbf{V}}_i^{(0)}$ based on (14). At the nth iteration, based on $\widehat{\mathbf{V}}_i^{(n-1)}$, we can get $\boldsymbol{\lambda}^{(n-1)}$ via Algorithm 1. Then, we solve problem (30) via Algorithm 2, and update $\widehat{\mathbf{V}}_i^{(n)}=\mathbf{V}_i^{(n-1)}$ until two consecutive user pairing vectors are the same, i.e., $\boldsymbol{\lambda}^{(n)}=\boldsymbol{\lambda}^{(n+1)}$. Finally, the power allocation coefficients are obtained via Algorithm 3. The details of the alternating beamforming algorithm are summarized in Algorithm 4. Due to the highly coupled between user pairing and STAR-RIS phase shift design, and the SCA procedure, our proposed alternating beamforming algorithm only can obtain high quality suboptimal solutions (will be verified in section VI), while the global optimal solution can only be found through exhaustively searching over all possibilities of STAR-RIS beamforming, transmit beamforming, power allocation coefficients, and user pairing vector, which is computationally prohibitive. As a result, the total complexity of Algorithm 4 is $\mathcal{O}\Big(\big(K^3+((6K+3)(M+1)^{\frac{7}{2}}+(6K+1+S)^3(N+1)^{\frac{1}{2}})L_1\log(\epsilon_1^{-1})\big)L_3\Big)$, where L_3 is the number of iterations of Algorithm 4.

V. Approximated Solution of the Statistical Eavesdropping CSI Scheme

In this section, we first derive the exact SOP of the legitimate users given the user pairing vector. Then, modified iterative algorithm is developed for jointly optimizing the beamforming vectors. Finally, an alternating beamforming algorithm is proposed to solve the problem (11).

A. Exact SOP

We first consider the user pairing vector $\boldsymbol{\lambda}$. The user pairing subproblem for the statistical eavesdropping CSI scheme in (11) can be reformulated as

$$\min_{\boldsymbol{\lambda}} \quad \max_{s\in\mathcal{S},i\in\mathcal{I},k\in\mathcal{K}} \lambda_{s,i,k}P_{s,i,k}^{SOP} \tag{34a}$$

$$\text{s.t.} \quad \text{(10f)}. \tag{34b}$$

As the full CSI of all the legitimate channels is perfectly available at the BS, the problem (34) can be solved by Algorithm 1. After user pairing, the SOP of the legitimate user in region i on sub-carrier s can be equivalently transformed into

$$P_{s,i}^{SOP}=\mathbb{P}\Bigg(\frac{(2^{R_{u,s,i}^{min}-\widetilde{R}_{s,i}^{sec}}-1)\sigma^2}{\rho_{s,i}\varrho^2 d_{RE}^{-\alpha_{RE}}d_{BR}^{-\alpha_{BR}}} < \left|\frac{\mathbf{h}_{e,i}^H\boldsymbol{\Theta}_i\mathbf{G}_s\mathbf{w}_s}{\varrho\sqrt{d_{RE}^{-\alpha_{RE}}}\sqrt{d_{BR}^{-\alpha_{BR}}}}\right|^2\Bigg), \tag{35}$$

where ϱ denotes the path loss at the reference distance of 1 meter, d_{RE} and d_{BR} denote the distances from the STAR-RIS to the PE in region i and from the BS to the STAR-RIS, respectively, as well as α_{RE} and α_{BR} denote the path loss exponents of the transmission from the STAR-RIS to the PE and from the BS to the STAR-RIS, respectively.

Define $\Omega_{e,s,i}=\frac{\mathbf{h}_{e,i}^H\boldsymbol{\Theta}_i\mathbf{G}_s\mathbf{w}_s}{\varrho\sqrt{d_{RE}^{-\alpha_{RE}}}\sqrt{d_{BR}^{-\alpha_{BR}}}}=\sum_{n=1}^{N}\sum_{m=1}^{M}\bar{h}_{e,i_m}^H\sqrt{\beta_i^m}e^{j\phi_i^m}\bar{G}_{s_{m,n}}\bar{w}_{s_n}$, $\forall s\in\mathcal{S}$ and $\forall i\in\mathcal{I}$, where $\bar{h}_{e,i_m}$, $\bar{G}_{s_{m,n}}$ and $\bar{w}_{s_n}$ denote the small fading coefficients. To compute the distribution of the random variables $\Omega_{e,s,i}$, we derive the exact probability density function (PDF) of $\delta_{e,s,i}^{n,m}=\bar{h}_{e,i_m}^H\sqrt{\beta_i^m}e^{j\phi_i^m}\bar{G}_{s_{m,n}}(1\le n\le N,1\le m\le M)$. Consider $\bar{h}_{e,i_m}=a_m-jb_m$, $\sqrt{\beta_i^m}e^{j\phi_i^m}=\sqrt{\beta_i^m}(\cos\phi_i^m+i\sin\phi_i^m)$ and $\bar{G}_{s_{m,n}}=c_m+jd_m$, where the real random variables a_m, b_m, c_m and d_m are independent and identically distributed (i.i.d.) Gaussian random variables, i.e., a_m, b_m, c_m, $d_m\sim\mathcal{CN}(0,\frac{1}{2})$ [38]. Therefore, we can rewrite $\delta_{e,s,i}^{n,m}$ as

$$\delta_{e,s,i}^{n,m}=\sqrt{\beta_i^m}\Big(\underbrace{a_m\bar{c}_m+b_m\bar{d}_m}_{e_m}+j\underbrace{(a_m\bar{d}_m-b_m\bar{c}_m)}_{f_m}\Big), \tag{36}$$

where $\bar{c}_m=\cos\phi_i^m c_m-\sin\phi_i^m d_m$ and $\bar{d}_m=\sin\phi_i^m c_m+\cos\phi_i^m d_m$. By treating c_m, d_m and ϕ_i^m as constant coefficients, e_m and f_m are i.i.d. Gaussian random variables, i.e., e_m, $f_m\sim\mathcal{CN}(0,\frac{\bar{c}_m^2+\bar{d}_m^2}{2})$ [38]. Therefore, the complex variable $\delta_{e,s,i}^{n,m}$ has a complex Gaussian distribution, i.e., $\delta_{e,s,i}^{n,m}\sim\mathcal{CN}(0,\beta_i^m(\bar{c}_m^2+\bar{d}_m^2))$, where $\bar{c}_m^2+\bar{d}_m^2=c_m^2+d_m^2=|\bar{G}_{s_{m,n}}|^2$. Furthermore, consider $\bar{w}_{s_n}=g_n-jh_n$, where g_n and h_n are i.i.d. Gaussian random variables. Therefore, $\Omega_{e,s,i}^{n,m}$ can be expressed as

$$\begin{aligned}\Omega_{e,s,i}^{n,m}&=\delta_{e,s,i}^{n,m}\bar{w}_{s_n}\\&=\sqrt{\beta_i^m}(e_m+jf_m)(g_n-jh_n)\\&=\sqrt{\beta_i^m}\Big(\underbrace{e_mg_n+f_mh_n}_{p_m}+j\underbrace{(f_mg_n-e_mh_n)}_{q_m}\Big).\end{aligned} \tag{37}$$

Similarly, by treating g_n and h_n as constant coefficients, p_m and q_m are i.i.d. Gaussian random variables, i.e., p_m, $q_m\sim\mathcal{CN}(0,\frac{(g_n^2+h_n^2)(\bar{c}_m^2+\bar{d}_m^2)}{2})$. The complex variable $\Omega_{e,s,i}^{n,m}$ has a complex Gaussian distribution, i.e., $\Omega_{e,s,i}^{n,m}\sim\mathcal{CN}(0,\beta_i^m(g_n^2+h_n^2)(\bar{c}_m^2+\bar{d}_m^2))$, where $g_n^2+h_n^2=|\bar{w}_{s_n}|^2$. Finally, by summing the real parts and imaginary parts, we have $\Omega_{e,s,i}\sim\mathcal{CN}(0,\sum_{n=1}^{N}\sum_{m=1}^{M}\beta_i^m|\bar{w}_{s_n}|^2|\bar{G}_{s_{m,n}}|^2)$. Note that the PDF of $|\Omega_{e,s,i}|^2$ is an function of exponential distribution with parameter $\frac{1}{\sum_{n=1}^{N}\sum_{m=1}^{M}\beta_i^m|\bar{w}_{s_n}|^2|\bar{G}_{s_{m,n}}|^2}$, $\forall s\in\mathcal{S},\forall i\in\mathcal{I}$.

As a result, the exact SOP of the legitimate user in (35) in region i on sub-carrier s can be expressed as

$$\begin{aligned}P_{s,i}^{SOP}&=\mathbb{P}\Bigg(\frac{(2^{R_{u,s,i}^{min}-\widetilde{R}_{s,i}^{sec}}-1)\sigma^2}{\rho_{s,i}\varrho^2 d_{RE}^{-\alpha_{RE}}d_{BR}^{-\alpha_{BR}}}<|\Omega_{e,s,i}|^2\Bigg)\\&=\int_{\frac{(2^{R_{u,s,i}^{min}-\widetilde{R}_{s,i}^{sec}}-1)\sigma^2}{\rho_{s,i}\varrho^2 d_{RE}^{-\alpha_{RE}}d_{BR}^{-\alpha_{BR}}}}^{\infty}\eta e^{-\eta|\Omega_{e,s,i}|^2}\mathrm{d}|\Omega_{e,s,i}|^2\\&=e^{-\frac{(2^{R_{u,s,i}^{min}-\widetilde{R}_{s,i}^{sec}}-1)\sigma^2\eta}{\rho_{s,i}\varrho^2 d_{RE}^{-\alpha_{RE}}d_{BR}^{-\alpha_{BR}}}},\end{aligned} \tag{38}$$

where $\eta=\frac{1}{\sum_{n=1}^{N}\sum_{m=1}^{M}\beta_i^m|\bar{w}_{s_n}|^2|\bar{G}_{s_{m,n}}|^2}$.

Algorithm 5 Alternating Beamforming Algorithm for Solving Problem (11)

1: **Initialization:**
Initialize the passive beamforming $\widehat{\mathbf{V}}_i^{(0)}$ according to (14). Set $n = 1$.
2: **repeat**
3: Compute $\boldsymbol{\lambda}^{(n-1)}$ via **Algorithm 1**.
4: Compute $\mathbf{V}_i^{(n-1)}$ by solving problem (43).
5: Update $\widehat{\mathbf{V}}_i^{(n)} = \mathbf{V}_i^{(n-1)}$.
6: $n = n + 1$.
7: **until** Two consecutive user pairing vectors are the same.
8: Optimize the power allocation coefficients by solving problem (44).

B. Joint Beamforming and Power Allocation Optimization

Optimizing the beamforming with fixed power allocation: Based on (13), (38), problem (11) simplifies to the following subproblem of joint beamforming optimization

$$\min_{\mathbf{V}_t,\mathbf{V}_r,\mathbf{W}_s,p} \quad p \tag{39a}$$

$$\text{s.t.} \frac{\rho_{s,i} d_{RE}^{-\alpha_{RE}} d_{BR}^{-\alpha_{BR}} \sum_{n=1}^{N}\sum_{m=1}^{M} \mathbf{V}_i(m,m)\mathrm{Tr}(\mathbf{W}_s)|\bar{G}_{s_{m,n}}|^2}{2^{R_{u,s,i}^{min}-\tilde{R}_{s,i}^{sec}}-1} \leq p, \tag{39b}$$

$$(16b)-(16h), \tag{39c}$$

where $p \geq 0$. Note that the constraints (16b), (16c) and (16d) can be transformed into convex forms in (21), (22) and (23), respectively. Therefore, we focus on handling the constraint (39b).

By introducing the auxiliary variable h, (39b) can be rewritten as

$$\frac{\rho_{s,i} d_{RE}^{-\alpha_{RE}} d_{BR}^{-\alpha_{BR}} \sum_{n=1}^{N}\sum_{m=1}^{M} \mathbf{V}_i(m,m)\mathrm{Tr}(\mathbf{W}_s)|\bar{G}_{s_{m,n}}|^2}{(2^{R_{u,s,i}^{min}-\tilde{R}_{s,i}^{sec}}-1)} \leq h^2, \tag{40}$$

and

$$h^2 \leq p. \tag{41}$$

Note that (40) can be transformed into an LMI, which is a convex constraint and is given by

$$\begin{bmatrix} \frac{\rho_{s,i} d_{RE}^{-\alpha_{RE}} d_{BR}^{-\alpha_{BR}} \sum_{n=1}^{N}\sum_{m=1}^{M} \mathbf{V}_i(m,m)|\bar{G}_{s_{m,n}}|^2}{(2^{R_{u,s,i}^{min}-\tilde{R}_{s,i}^{sec}}-1)} & h \\ h & \mathrm{Tr}(\mathbf{W}_s) \end{bmatrix} \succeq 0. \tag{42}$$

As a result, problem (39) can be reformulated as follows:

$$\min_{\substack{\mathbf{V}_t,\mathbf{V}_r,\mathbf{W}_s,p,h,\\ \bar{L}_{u,s,i},\underline{L}_{u,s,i}}} \quad p \tag{43a}$$

$$\text{s.t.} \quad (16e)-(16h), (19)-(23), (41), (42). \tag{43b}$$

Problem (43) is convex and can be solved by using Algorithm 2.

Optimizing power allocation with fixed beamforming: With fixed $\{\mathbf{V}_i\}_{i\in\mathcal{I}}$ and $\{\mathbf{W}_s\}_{s\in\mathcal{S}}$, the subproblem of optimizing the power allocation coefficients is formulated as

$$\min_{\boldsymbol{\rho}} \quad \max_{s\in\mathcal{S},i\in\mathcal{I}} \varsigma_{s,i} \tag{44a}$$

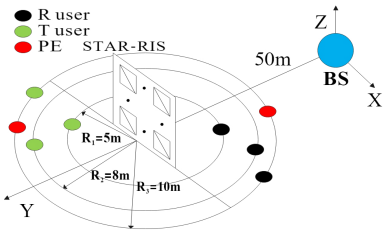

Fig. 3. Simulation setup of the STAR-RIS assisted downlink NOMA network.

$$\text{s.t.} \quad (16b)-(16d), (16h), (31c), \tag{44b}$$

where $\varsigma_{s,i}$ is a linear function with respect to $\rho_{s,i}$, i.e., $\varsigma_{s,i} = \frac{\rho_{s,i} d_{RE}^{-\alpha_{RE}} d_{BR}^{-\alpha_{BR}} \sum_{n=1}^{N}\sum_{m=1}^{M} \mathbf{V}_i(m,m)\mathrm{Tr}(\mathbf{W}_s)|\bar{G}_{s_{m,n}}|^2}{(2^{R_{u,s,i}^{min}-\tilde{R}_{s,i}^{sec}}-1)}$. Note that problem (44) is a linear programming problem. Therefore, it can be efficiently solved by CVX.

C. Overall Algorithm

In order to obtain the beamforming vectors, we develop an alternating beamforming algorithm for solving problem (11). The alternating beamforming algorithm is summarized in Algorithm 5. The main computational complexity of Algorithm 5 relies on the complexitys of Algorithm 1 and solving problem (43). As a result, the total complexity of Algorithm 5 is $\mathcal{O}\Big(\big(K^3 + ((6K+3)(M+1)^{\frac{7}{2}} + (6K+1+S)^3(N+1)^{\frac{1}{2}})L_1\log(\epsilon_1^{-1})\big)L_4\Big)$, where L_4 is the number of iterations of Algorithm 5.

VI. Simulation Results and Discussion

In this section, the secrecy performance of the proposed STAR-RIS-NOMA network is evaluated by numerical simulations. As shown in Fig. 3, we consider a three dimensional coordinate network, where the BS is located at the origin (i.e., (0, 0, 0) in meter (m)) and the STAR-RIS is placed perpendicular to the ground (i.e., x-y plane). The STAR-RIS is assumed to be equipped with a uniform planar array, whose reference center is located at (0, 50, 0) m. The three legitimate users in each region (i.e., $K = 3$) are distributed on a circle centered at the STAR-RIS with a radius of $R_1 = 5$ m, $R_2 = 8$ m and $R_3 = 10$ m, respectively, while the PE in each region is distributed on a circle centered at the STAR-RIS whose radius is $R_3 = 10$ m. Moreover, the Rician fading channel from the STAR-RIS to the user in region i on sub-carrier s is given by

$$\mathbf{h}_{u,s,i} = \sqrt{\varrho d_{R,s,i}^{-\alpha_{RU}}}\left(\sqrt{\frac{\kappa}{\kappa+1}}\hat{\mathbf{h}}_L + \sqrt{\frac{1}{\kappa+1}}\hat{\mathbf{h}}_R\right), \tag{45}$$

where $d_{R,s,i}$ denotes the distance from the STAR-RIS to the user in region i on sub-carrier s, α_{RU} is the path loss exponent, κ is the Rician factor, $\hat{\mathbf{h}}_L$ and $\hat{\mathbf{h}}_R$ denote the deterministic line-of-sight (LoS) channel component and the non-line-of-sight (NLoS) component modeled as Rayleigh fading, respectively. The channel fading from the BS to the STAR-RIS, and from the STAR-RIS to the PE, can be similarly modeled according to (45). In addition, we set $\alpha_{BR} = 2.2$, $\alpha_{RU} = \alpha_{RE} = 2.5$, $\varrho = 10^{-3}$, $\sigma^2 = -60$ dBm, and the target rate and the target secrecy rate at all legitimate users are assumed to be the same, i.e., $R_{u,s,i,k}^{min} = R^{min}$, $\tilde{R}_{s,i,k}^{sec} = \tilde{R}^{sec}$, $\forall s \in \mathcal{S}, \forall i \in \mathcal{I}, \forall k \in \mathcal{K}$.

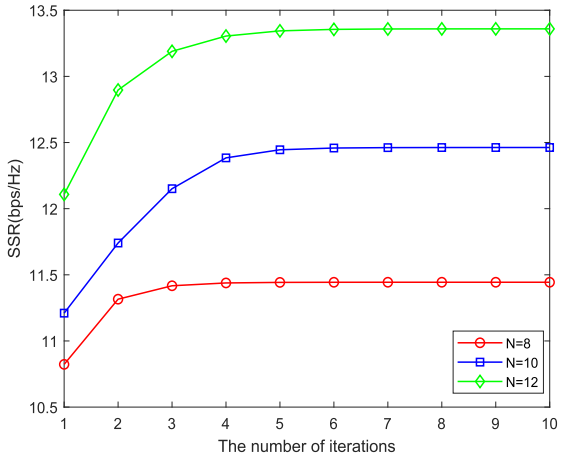

(a) Convergence behavior of Algorithm 3 for the full CSI of the PE's channel, where $M = 20$, $\kappa = 3$, $R^{min} = 1$ bps/Hz and $P_{max} = 40$ dBm.

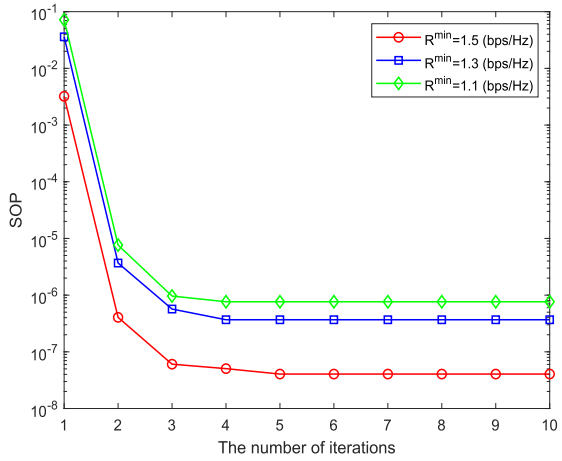

(b) Convergence behavior of Algorithm 2 for the statistical CSI of the PE's channel, where $M = 20$, $N = 8$, $\kappa = 0$, $\widetilde{R}^{sec} = 0.1$bps/Hz and $P_{max} = 40$ dBm.

Fig. 4. Convergence behavior of the proposed algorithms.

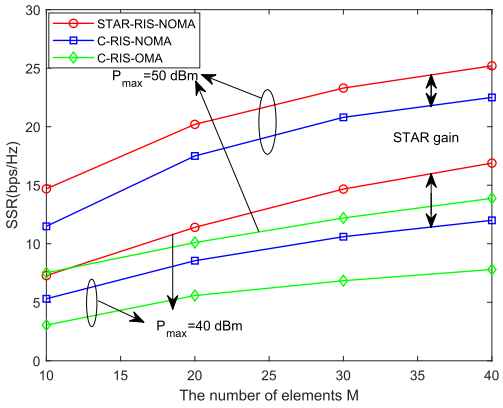

(a) The SSR versus the number of elements M with different total transmit power P_{max} under the full CSI of the PE's channel, where $N = 8$, $\kappa = 3$ and $R^{min} = 1$ bps/Hz.

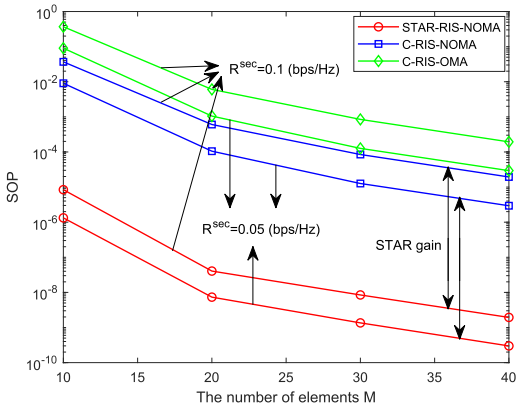

(b) The maximum SOP versus the number of elements M with different target secrecy rate $\widetilde{R}^{sec}$ under the statistical CSI of the PE's channel, where $N = 8$, $\kappa = 0$, $R^{min} = 1.5$ bps/Hz and $P_{max} = 40$ dBm.

Fig. 5. Comparison of the performance of the proposed STAR-RIS-NOMA, with C-RIS-NOMA and C-RIS-OMA.

A. Convergence Behavior of the Proposed Algorithms

The convergence of the proposed algorithms is illustrated in Fig. 4, where both algorithms converge quickly, i.e., within 10 iterations. Furthermore, in Fig. 4(a), it can be observed that the SSR of STAR-RIS-NOMA improves as the number of the antennas N increases, since the active beamfoming gain improves when increasing N. In addition, in Fig. 4(b), it can be observed that the SOP of STAR-RIS-NOMA decreases as R^{min} increases. Although the increase of R^{min} will improve the reception ability of PE, it also increases the redundant rate. This result shows that with the increase of R^{min}, the gain of redundant rate becomes greater than that of PE reception ability.

B. Performance Comparison of the Proposed Schemes

To demonstrate the performance of the proposed scheme, we consider the following benchmark schemes:

- **C-RIS-NOMA:** In this scheme, one traditional reflecting-only RIS and one transmitting-only RIS are deployed adjacently at the same location of the STAR-RIS to achieve full-space coverage [17]. Then, the users on a region are served over the same time and frequency resource block. Furthermore, for a fair comparison, each C-RIS is equipped with $\frac{M}{2}$ elements. As a heuristic scheme for STAR-RIS gain with phase shift design, this benchmark scheme can be regarded as a special case of an STAR-RIS MS mode, where $\frac{M}{2}$ elements operate in the T mode and $\frac{M}{2}$ elements operate in the R mode.
- **C-RIS-OMA:** In this scheme, the deployment and elements of C-RIS are the same as those of C-RIS-NOMA. While, the users on a region are served by time division multiple access to avoid co-carrier interference.

Fig. 5 shows the secrecy performance of the proposed STAR-RIS-NOMA network under the full CSI and statistical CSI for the PE's channel, respectively. It can be observed from Fig. 5(a) and Fig. 5(b) that the secrecy performance of the proposed STAR-RIS-NOMA is better than C-RIS-NOMA and C-RIS-OMA. This is because STAR-RIS can unleash more adjustment DoFs than C-RIS. More specifically, STAR-RIS has independently adjustable surface's electrical impedance and magnetic impedance, which is capable of controling the amplitudes and phase shifts of transmitted and reflected signals. Furthermore, the secrecy performance of C-RIS-NOMA outperforms C-RIS-OMA, since NOMA allows the legitimate users to transmit their signals on the same time-frequency resource block. In addition, the secrecy performance of all schemes improves as the number of elements M increases.

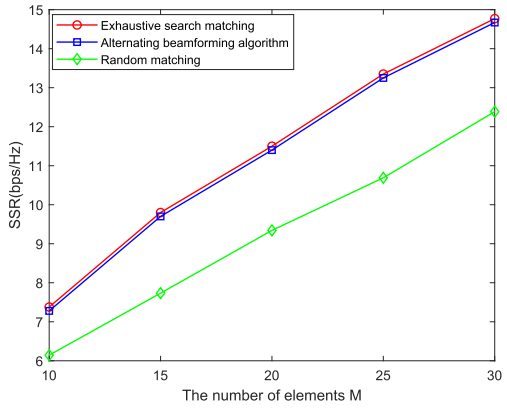

(a) The SSR versus the number of elements M with $N = 8$, $\kappa = 3$, $R^{min} = 1$ bps/Hz and $P_{max} = 40$ dBm under the full CSI of the PE's channel.

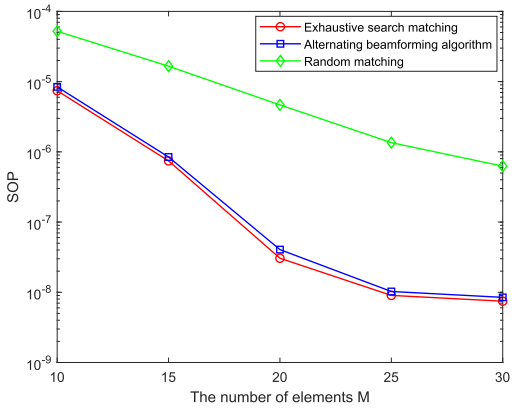

(b) The maximum SOP versus the number of elements M with $N = 8$, $\kappa = 0$, $R^{min} = 1.5$ bps/Hz, $\widetilde{R}^{sec} = 0.1$bps/Hz and $P_{max} = 40$ dBm under the statistical CSI of the PE's channel.

Fig. 6. The impact of the proposed alternating beamforming algorithm on the secrecy performance of the STAR-RIS-NOMA networks.

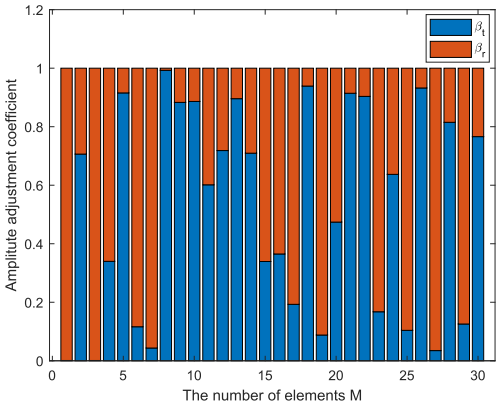

(a) Amplitude adjustment of the transmitted and reflected signals by each element for the full CSI of the PE's channel, where $N = 8$, $\kappa = 3$, $R^{min} = 1$ bps/Hz and $P_{max} = 40$ dBm.

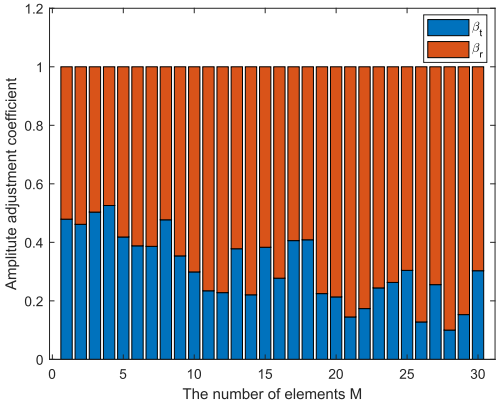

(b) Amplitude adjustment of the transmitted and reflected signals by each element for the statistical CSI of the PE's channel, where $N = 8$, $\kappa = 0$, $R^{min} = 1.5$ bps/Hz, $\widetilde{R}^{sec} = 0.1$bps/Hz and $P_{max} = 40$ dBm.

Fig. 7. The values of the transmission and reflection amplitudes for each STAR-RIS element.

This is because more elements M can provide higher passive beamforming gain, which enhances the security. However, the computational complexity of the proposed algorithms grows significantly as the number of elements M increase. Therefore, the choice of the number of RIS elements should achieve a tade-off between the secrecy performance and the computational complexity.

Furthermore, we observe from Fig. 5(a) that the SSR of all schemes improves as P_{max} increases. The main reason is that more power will be allocated to the legitimate users with the increase of P_{max}, which leads to the improvement of the SSR. Moreover, as P_{max} increases, the SSR gain of both STAR-RIS-NOMA and C-RIS-NOMA are much greater than that of C-RIS-OMA. It is because the multiple access gain of NOMA brought by the power domain multiplexing is significantly improved in the high power regime [32]. Note that in Fig. 5(b), the SOP of all schemes decreases as $\widetilde{R}^{sec}$ decreases. The main reason is that more redundant rate will be used to against PE with the decrease of $\widetilde{R}^{sec}$, which leads to the improvement of the secrecy performance for the three schemes.

C. Impact of User Pairing

To evaluate the effectiveness of the proposed alternating beamforming algorithm, two benchmarks are provided in this subsection. The first benchmark, called exhaustive search matching [17], finds the optimal user pairing vector via exhaustive search. The second benchmark, which is referred to as random matching, selects the user pairing vector randomly. Fig. 6 plots the secrecy performance of the alternating beamforming algorithm, exhaustive search matching, and random matching under the full CSI and the statistical CSI of the PE's channel, respectively.

It is observed from Fig. 6(a) and Fig. 6(b) that the proposed alternating beamforming algorithm can achieve nearly the same secrecy performance as the exhaustive search matching [17]. This demonstrates the effectiveness of the proposed alternating beamforming algorithm. The main reason is that the KM algorithm is to maximize the difference of the channel gains between the paired users in the same sub-carrier, and the performance of the NOMA scheme will be improved accordingly [42]. Furthermore, from Fig. 6(a), we can observe that the SSR of the proposed alternating beamforming algorithm is higher than that of the random matching. This is because the alternating beamforming algorithm can maximize the differences of users' channel gains in the sub-carriers, thus reducing the interference suffered by weak users in each sub-carrier. In addition, note that in Fig. 6(b), the SOP of the alternating beamforming algorithm is lower than that of the random matching. This is because the alternating beamforming

$$\sum_{s=1}^{S}\sum_{i\in\mathcal{I}} R_{s,i}^{sec}$$
$$= \sum_{s=1}^{S}\Bigg[\log_2\left(1+\frac{\rho_{s,t}\Lambda_{u,s,t}}{\psi_{s,t}\rho_{s,r}\Lambda_{u,s,t}+\sigma^2}\right)-\log_2\left(1+\frac{\rho_{s,t}\Lambda_{e,s,t}}{\sigma^2}\right)+\log_2\left(1+\frac{\rho_{s,r}\Lambda_{u,s,r}}{\psi_{s,r}\rho_{s,t}\Lambda_{u,s,r}+\sigma^2}\right)$$
$$-\log_2\left(1+\frac{\rho_{s,r}\Lambda_{e,s,r}}{\sigma^2}\right)\Bigg] = \sum_{s=1}^{S}\Bigg[\underbrace{\log_2\left(\rho_{s,t}\Lambda_{u,s,t}+\psi_{s,t}\rho_{s,r}\Lambda_{u,s,t}+\sigma^2\right)+\log_2\left(\sigma^2\right)}_{\chi_{u,s,t}}\underbrace{-\log_2\left(\psi_{s,t}\rho_{s,r}\Lambda_{u,s,t}+\sigma^2\right)}_{\varpi_{u,s,t}}$$
$$\underbrace{-\log_2\left(\rho_{s,t}\Lambda_{e,s,t}+\sigma^2\right)}_{\varpi_{e,s,t}}\underbrace{+\log_2\left(\rho_{s,r}\Lambda_{u,s,r}+\psi_{s,r}\rho_{s,t}\Lambda_{u,s,r}+\sigma^2\right)+\log_2\left(\sigma^2\right)}_{\chi_{u,s,r}}\underbrace{-\log_2\left(\psi_{s,r}\rho_{s,t}\Lambda_{u,s,r}+\sigma^2\right)}_{\varpi_{u,s,r}}$$
$$\underbrace{-\log_2\left(\rho_{s,r}\Lambda_{e,s,r}+\sigma^2\right)}_{\varpi_{e,s,r}}\Bigg] \geq q. \tag{46}$$

algorithm can reduce the interference suffered by the weakest user, which implies that the weakest user can use less power to achieve the QoS requirements than that achieved by the random matching.

D. Allocation of the Transmission and Reflection Amplitudes

To observe the energy allocation in the transmission and reflection regions, Fig. 7 plots the transmission and reflection amplitudes for each STAR-RIS element under the full CSI and the statistical CSI of the PE's channel, respectively. From Fig. 7(a), we can observe that the energy allocated to the transmission amplitudes is roughly the same as that allocated to the reflection amplitudes. This is expected because the channel gains of the users in the two regions are almost the same. Thus, STAR-RIS evenly allocates energy to the two regions. Furthermore, from Fig. 7(b), we see that the energy allocated to the reflection amplitudes are more than that allocated to the transmission amplitudes. This phenomenon can be explained considering that the weakest user can be located in the reflection region. In this context, to fulfill the QoS requirement, STAR-RIS have to allocate more energy to the reflection amplitudes.

VII. Conclusion

In this paper, we investigated the secrecy performance for a downlink multi-carrier NOMA network, in which STAR-RIS was employed to relay the superimposed information of BS to the legitimate receiver, while suppressing malicious eavesdropping. The SSR maximization problem and the maximum SOP minimization problem were proposed for the full CSI and statistical CSI of the PE's channel, respectively. For tackling these optimization problems, we developed alternating beamforming algorithms by jointly designing the transmission and reflection beamforming of the STAR-RIS, the transmit beamforming of the BS, the power allocation coefficients, and the user pairing vector. Specifically, for the full eavesdropping CSI, we firstly proposed a KM algorithm based on the differences of user's channel gains to optimize the user pairing vector. Then, we optimized the beamforming vectors and power allocation coefficients step-by-step using SDP and SLB approximate. Furthermore, for the statistical eavesdropping CSI, the exact SOP was derived, where the LMI was used to reformulated non-convex constraints. Simulation results illustrated that the proposed STAR-RIS-NOMA scheme outperforms the existing C-RIS-NOMA scheme and C-RIS-OMA scheme, and revealed the effectiveness of the user pairing designs.

In this work, we assume that the phase shift coefficients for transmission and reflection can be independently adjusted. However, in the practical communication scenarios, the phase shift coefficients for transmission and reflection may be coupled due to the pure passivity of STAR-RIS, which will not only cause performance degradation but also make the user pairing much more complicated. Therefore, the above situation will be the focus of our future research work.

Appendix

Firstly, the constraint (31b) can be rewritten as given in (46) at the top of this page. From convex optimization theory, the constraint (31b) is a convex function when the left hand side of constraint (31b) is a concave function. To this end, we use the SLB to approximate the non-convex terms $\{\varpi_{u,s,i}, \varpi_{e,s,i}\}_{s\in\mathcal{S},i\in\mathcal{I}}$ [41]. By invoking the SLB, the non-concave functions $\varpi_{u,s,i}$ and $\varpi_{e,s,i}$, for $s\in\mathcal{S}, i\in\mathcal{I}$ can be expressed as:

$$\varpi_{u,s,i} = -\frac{a_{u,s,i}}{\ln 2}\left(\psi_{s,i}\rho_{s,i'}\Lambda_{u,s,i}+\sigma^2\right)+\log_2 a_{u,s,i}+\frac{1}{\ln 2},$$
$$\varpi_{e,s,i} = -\frac{a_{e,s,i}}{\ln 2}\left(\rho_{s,i}\Lambda_{e,s,i}+\sigma^2\right)+\log_2 a_{e,s,i}+\frac{1}{\ln 2}, \tag{47}$$

where $i\neq i', i, i'\in\mathcal{I}$, $a_{u,s,i} = \frac{1}{\psi_{s,i}\rho_{s,i'}\Lambda_{u,s,i}+\sigma^2}$ and $a_{e,s,i} = \frac{1}{\rho_{s,i}\Lambda_{e,s,i}+\sigma^2}$.

According to (47), the constraint (31b) can be rewritten as (32). The proof is completed.

References

[1] P. Yang, Y. Xiao, M. Xiao, and S. Li, "6G wireless communications: Vision and potential techniques," *IEEE Netw.*, vol. 33, no. 4, pp. 70–75, Jul./Aug. 2019.

[2] W. Saad, M. Bennis, and M. Chen, "A vision of 6G wireless systems: Applications, trends, technologies, and open research problems," *IEEE Netw.*, vol. 34, no. 3, pp. 134–142, May/Jun. 2020.

[3] Q. Wu and R. Zhang, "Towards smart and reconfigurable environment: Intelligent reflecting surface aided wireless network," *IEEE Commun. Mag.*, vol. 58, no. 1, pp. 106–112, Jan. 2020.

[4] M. A. El Mossallamy, H. Zhang, L. Song, K. G. Seddik, Z. Han, and G. Y. Li, "Reconfigurable intelligent surfaces for wireless communications: Principles, challenges, and opportunities," *IEEE Trans. Cognit. Commun. Netw.*, vol. 6, no. 3, pp. 990–1002, Sep. 2020.

[5] M. Di Renzo et al., "Smart radio environments empowered by reconfigurable intelligent surfaces: How it works, state of research, and the road ahead," *IEEE J. Sel. Areas Commun.*, vol. 38, no. 11, pp. 2450–2525, Nov. 2020.

[6] Z. Ding, X. Lei, G. K. Karagiannidis, R. Schober, J. Yuan, and V. K. Bhargava, "A survey on non-orthogonal multiple access for 5G networks: Research challenges and future trends," *IEEE J. Sel. Areas Commun.*, vol. 35, no. 10, pp. 2181–2195, Oct. 2017.

[7] Y. Liu, Z. Qin, M. Elkashlan, Z. Ding, A. Nallanathan, and L. Hanzo, "Nonorthogonal multiple access for 5G and beyond," *Proc. IEEE*, vol. 105, no. 12, pp. 2347–2381, Dec. 2017.

[8] G. Yang, X. Xu, Y.-C. Liang, and M. D. Renzo, "Reconfigurable intelligent surface-assisted non-orthogonal multiple access," *IEEE Trans. Wireless Commun.*, vol. 20, no. 5, pp. 3137–3151, May 2021.

[9] Y. Liu, X. Mu, X. Liu, M. Di Renzo, Z. Ding, and R. Schober, "Reconfigurable intelligent surface-aided multi-user networks: Interplay between NOMA and RIS," *IEEE Wireless Commun.*, vol. 29, no. 2, pp. 169–176, Apr. 2022.

[10] X. Xie, F. Fang, and Z. Ding, "Joint optimization of beamforming, phase-shifting and power allocation in a multi-cluster IRS-NOMA network," *IEEE Trans. Veh. Technol.*, vol. 70, no. 8, pp. 7705–7717, Aug. 2021.

[11] Y. Xiu et al., "Reconfigurable intelligent surfaces aided mmWave NOMA: Joint power allocation, phase shifts, and hybrid beamforming optimization," *IEEE Trans. Wireless Commun.*, vol. 20, no. 12, pp. 8393–8409, Dec. 2021.

[12] Q. Wu, S. Zhang, B. Zheng, C. You, and R. Zhang, "Intelligent reflecting surface-aided wireless communications: A tutorial," *IEEE Trans. Commun.*, vol. 69, no. 5, pp. 3313–3351, May 2021.

[13] J. Xu, Y. Liu, X. Mu, and O. A. Dobre, "STAR-RISs: Simultaneous transmitting and reflecting reconfigurable intelligent surfaces," *IEEE Commun. Lett.*, vol. 25, no. 9, pp. 3134–3138, Sep. 2021.

[14] T. Wang, M.-A. Badiu, G. Chen, and J. P. Coon, "Performance analysis of IOS-assisted NOMA system with channel correlation and phase errors," *IEEE Trans. Veh. Technol.*, vol. 71, no. 11, pp. 11861–11875, Nov. 2022.

[15] C. Pfeiffer and A. Grbic, "Metamaterial Huygens' surfaces: Tailoring wave fronts with reflectionless sheets," *Phys. Rev. Lett.*, vol. 110, no. 19, May 2013, Art. no. 197401.

[16] J. Zuo, Y. Liu, Z. Ding, L. Song, and H. V. Poor, "Joint design for simultaneously transmitting and reflecting (STAR) RIS assisted NOMA systems," *IEEE Trans. Wireless Commun.*, vol. 22, no. 1, pp. 611–626, Jan. 2023.

[17] C. Wu, X. Mu, Y. Liu, X. Gu, and X. Wang, "Resource allocation in STAR-RIS-aided networks: OMA and NOMA," *IEEE Trans. Wireless Commun.*, vol. 21, no. 9, pp. 7653–7667, Sep. 2022.

[18] Y. Zou, J. Zhu, X. Wang, and L. Hanzo, "A survey on wireless security: Technical challenges, recent advances, and future trends," *Proc. IEEE*, vol. 104, no. 9, pp. 1727–1765, Sep. 2016.

[19] A. D. Wyner, "The wire-tap channel," *Bell Syst. Tech. J.*, vol. 54, no. 8, pp. 1355–1387, Oct. 1975.

[20] M. Cui, G. Zhang, and R. Zhang, "Secure wireless communication via intelligent reflecting surface," *IEEE Wireless Commun. Lett.*, vol. 8, no. 5, pp. 1410–1414, Oct. 2019.

[21] G. Li, C. Sun, W. Xu, M. D. Renzo, and A. Hu, "On maximizing the sum secret key rate for reconfigurable intelligent surface-assisted multiuser systems," *IEEE Trans. Inf. Forensics Security*, vol. 17, pp. 211–225, 2022.

[22] H. Niu, Z. Chu, F. Zhou, and Z. Zhu, "Simultaneous transmission and reflection reconfigurable intelligent surface assisted secrecy MISO networks," *IEEE Commun. Lett.*, vol. 25, no. 11, pp. 3498–3502, Nov. 2021.

[23] S. Fang, G. Chen, Z. Abdullah, and Y. Li, "Intelligent omni surface-assisted secure MIMO communication networks with artificial noise," *IEEE Commun. Lett.*, vol. 26, no. 6, pp. 1231–1235, Jun. 2022.

[24] S. Fang, G. Chen, and Y. Li, "Joint optimization for secure intelligent reflecting surface assisted UAV networks," *IEEE Wireless Commun. Lett.*, vol. 10, no. 2, pp. 276–280, Feb. 2021.

[25] C. Huang, G. Chen, and K.-K. Wong, "Multi-agent reinforcement learning-based buffer-aided relay selection in IRS-assisted secure cooperative networks," *IEEE Trans. Inf. Forensics Security*, vol. 16, pp. 4101–4112, 2021.

[26] W. Wei, X. Pang, J. Tang, N. Zhao, X. Wang, and A. Nallanathan, "Secure transmission design for aerial IRS assisted wireless networks," *IEEE Trans. Commun.*, vol. 71, no. 6, pp. 3528–3540, Jun. 2023.

[27] X. Pang, N. Zhao, J. Tang, C. Wu, D. Niyato, and K.-K. Wong, "IRS-assisted secure UAV transmission via joint trajectory and beamforming design," *IEEE Trans. Commun.*, vol. 70, no. 2, pp. 1140–1152, Feb. 2022.

[28] H. Yang, Z. Xiong, J. Zhao, D. Niyato, L. Xiao, and Q. Wu, "Deep reinforcement learning-based intelligent reflecting surface for secure wireless communications," *IEEE Trans. Wireless Commun.*, vol. 20, no. 1, pp. 375–388, Jan. 2021.

[29] Z. Zhang, C. Zhang, C. Jiang, F. Jia, J. Ge, and F. Gong, "Improving physical layer security for reconfigurable intelligent surface aided NOMA 6G networks," *IEEE Trans. Veh. Technol.*, vol. 70, no. 5, pp. 4451–4463, May 2021.

[30] L. Yang and Y. Yuan, "Secrecy outage probability analysis for RIS-assisted NOMA systems," *Electron. Lett.*, vol. 56, no. 23, pp. 1254–1256, Nov. 2020.

[31] W. Wang et al., "Beamforming and jamming optimization for IRS-aided secure NOMA networks," *IEEE Trans. Wireless Commun.*, vol. 21, no. 3, pp. 1557–1569, Mar. 2022.

[32] Z. Zhang, J. Chen, Y. Liu, Q. Wu, B. He, and L. Yang, "On the secrecy design of STAR-RIS assisted uplink NOMA networks," *IEEE Trans. Wireless Commun.*, vol. 21, no. 12, pp. 11207–11221, Dec. 2022.

[33] Y. Han, N. Li, Y. Liu, T. Zhang, and X. Tao, "Artificial noise aided secure NOMA communications in STAR-RIS networks," *IEEE Wireless Commun. Lett.*, vol. 11, no. 6, pp. 1191–1195, Jun. 2022.

[34] X. Mu, Y. Liu, L. Guo, J. Lin, and R. Schober, "Simultaneously transmitting and reflecting (STAR) RIS aided wireless communications," *IEEE Trans. Wireless Commun.*, vol. 21, no. 5, pp. 3083–3098, May 2022.

[35] C. Wu, C. You, Y. Liu, X. Gu, and Y. Cai, "Channel estimation for STAR-RIS-aided wireless communication," *IEEE Commun. Lett.*, vol. 26, no. 3, pp. 652–656, Mar. 2022.

[36] L. Lv, Z. Ding, Q. Ni, and J. Chen, "Secure MISO-NOMA transmission with artificial noise," *IEEE Trans. Veh. Technol.*, vol. 67, no. 7, pp. 6700–6705, Jul. 2018.

[37] H.-M. Wang, X. Zhang, Q. Yang, and T. A. Tsiftsis, "Secure users oriented downlink MISO NOMA," *IEEE J. Sel. Topics Signal Process.*, vol. 13, no. 3, pp. 671–684, Jun. 2019.

[38] Z. Ding, R. Schober, and H. V. Poor, "On the impact of phase shifting designs on IRS-NOMA," *IEEE Wireless Commun. Lett.*, vol. 9, no. 10, pp. 1596–1600, Oct. 2020.

[39] Z.-Q. Luo, W.-K. Ma, A. M. So, Y. Ye, and S. Zhang, "Semidefinite relaxation of quadratic optimization problems," *IEEE Signal Process. Mag.*, vol. 27, no. 3, pp. 20–34, May 2010.

[40] M. Grant and S. Boyd. *CVX: MATLAB Software for Disciplined Convex Programming, Version 2.0 Beta*. Accessed: Sep. 2013. [Online]. Available: http://cvxr.com/cvx

[41] R. Feng, Q. Li, Q. Zhang, and J. Qin, "Robust secure beamforming in MISO full-duplex two-way secure communications," *IEEE Trans. Veh. Technol.*, vol. 65, no. 1, pp. 408–414, Jan. 2016.

[42] Z. Ding, P. Fan, and H. V. Poor, "Impact of user pairing on 5G nonorthogonal multiple-access downlink transmissions," *IEEE Trans. Veh. Technol.*, vol. 65, no. 8, pp. 6010–6023, Aug. 2016.

Yanbo Zhang received the B.S. degree in electronic information engineering from Minjiang University, Fuzhou, China, in 2019, and the M.S. degree in information and communication engineering from Fujian Normal University, Fuzhou, in 2023. His research interests include non-orthogonal multiple access, physical layer security, reconfigurable intelligent surface, and the applications of convex optimization in wireless communications.

Zheng Yang (Member, IEEE) received the Ph.D. degree in information and communications engineering from Southwest Jiaotong University, Chengdu, China, in 2016. He was a Visiting Ph.D. Student with the School of Electrical and Electronic Engineering, Newcastle University, Newcastle upon Tyne, U.K., in 2014. He is currently an Associate Professor with the College of Photonic and Electronic Engineering, Fujian Normal University. His research interests include reconfigurable intelligent surface, non-orthogonal multiple access, integrated sensing, and communications. He received the Excellent Doctoral Thesis Award from the China Education Society of Electronics in 2017, the IEEE Best Signal Processing Letter Award in 2018, and the Exemplary Reviewer Award of the IEEE WIRELESS COMMUNICATIONS LETTERS in 2022.

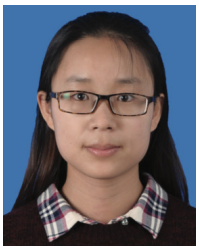

Jingjing Cui (Senior Member, IEEE) received the Ph.D. degree from Southwest Jiaotong University, Chengdu, China, in 2018. She was a Research Fellow with the School of Electronics and Computer Science, University of Southampton, U.K., and a Research Assistant with the School of Electronic Engineering and Computer Science, Queen Mary University of London, U.K., from 2018 to 2022. Her research interests include classical and quantum optimization theory and algorithm design, machine learning for wireless networks, and quantum communications. She received the Exemplary Reviewer of the IEEE TRANSACTIONS ON COMMUNICATIONS in 2019 and IEEE COMMUNICATION LETTERS in 2018. She has also served as a TPC Member for IEEE conferences, such as ICC and IEEE GLOBECOM.

Peng Xu (Member, IEEE) received the B.Eng. and Ph.D. degrees in electronic and information engineering from the University of Science and Technology of China, Anhui, China, in 2009 and 2014, respectively. From June 2014 to July 2016, he was a Post-Doctoral Researcher with the Department of Electronic Engineering and Information Science, University of Science and Technology of China, Hefei, China. He is currently an Associate Professor with the School of Communication and Information Engineering, Chongqing University of Posts and Telecommunications (CQUPT), Chongqing, China. His current research interests include cooperative communications, information-theoretic secrecy, NOMA techniques, and reconfigurable intelligent surface. He received the IEEE WIRELESS COMMUNICATIONS LETTERS Exemplary Reviewer in 2015 and 2021 and Excellent Paper of Chongqing Association for Science and Technology in 2018.

Gaojie Chen (Senior Member, IEEE) received the B.Eng. and B.Ec. degrees in electrical information engineering and international economics and trade from Northwest University, China, in 2006, and the M.Sc. (Hons.) and Ph.D. degrees in electrical and electronic engineering from Loughborough University, Loughborough, U.K., in 2008 and 2012, respectively. After graduation, he took up academic and research positions with DT Mobile, Loughborough University, University of Surrey, U.K., University of Oxford, U.K., and University of Leicester, U.K. He is currently an Assistant Professor with the Institute for Communication Systems, 5GIC & 6GIC, University of Surrey, and a Visiting Research Collaborator with the Information and Network Science Laboratory, University of Oxford. His current research interests include information theory, wireless communications, satellite communications, cognitive radio, the Internet of Things, secrecy communications, and random geometric networks. He received the Exemplary Reviewer Awards of the IEEE WIRELESS COMMUNICATIONS LETTERS in 2018, the IEEE TRANSACTIONS ON COMMUNICATIONS in 2019, and the IEEE COMMUNICATIONS LETTERS in 2020 and 2021; and an Exemplary Editor Awards of the IEEE COMMUNICATIONS LETTERS and IEEE WIRELESS COMMUNICATIONS LETTERS in 2021 and 2022, respectively. He served as an Associate Editor for the IEEE JOURNAL ON SELECTED AREAS IN COMMUNICATIONS—Machine Learning in Communications (2021–2022). He serves as an Associate Editor for the IEEE COMMUNICATIONS LETTERS, IEEE WIRELESS COMMUNICATIONS LETTERS, and *Electronics Letters* (IET).

Yi Wu (Member, IEEE) received the B.Eng. degree in radio technology from Southeast University, Nanjing, China, in 1991, the M.S. degree in communications and information systems from Fuzhou University, Fuzhou, China, in 2004, and the Ph.D. degree in information and communication engineering from Southeast University in 2013. She is currently a Professor with the College of Photonic and Electronic Engineering, Fujian Normal University. Her research interests include 5G networks, vehicular ad hoc networks, and communication protocols.

Marco Di Renzo (Fellow, IEEE) received the Laurea (cum laude) and Ph.D. degrees in electrical engineering from the University of L'Aquila, Italy, in 2003 and 2007, respectively, and the Habilitation Diriger des Recherches (Doctor of Science) degree from University Paris-Sud (currently Paris-Saclay University), France, in 2013. Currently, he is a CNRS Research Director (Professor) and the Head of the Intelligent Physical Communications Group, Laboratory of Signals and Systems (L2S), CNRS, CentraleSupelec, Paris-Saclay University, Paris, France. Also, he is an elected member of the L2S Board Council and a member of the L2S Management Committee. At Paris-Saclay University, he serves as the Coordinator of the Communications and Networks Research Area of the Laboratory of Excellence DigiCosme, a member of the Admission and Evaluation Committee of the Ph.D. School on Information and Communication Technologies, and a member of the Evaluation Committee of the Graduate School in Computer Science. He is a Founding Member and the Academic Vice Chair of the Industry Specification Group (ISG) on Reconfigurable Intelligent Surfaces (RIS) within the European Telecommunications Standards Institute (ETSI), where he serves as the Rapporteur for the work item on communication models, channel models, and evaluation methodologies. He is a fellow of the IET and AAIA; an Ordinary Member of the European Academy of Sciences and Arts, an Ordinary Member of the Academia Europaea; and a Highly Cited Researcher. Also, he holds the 2023 France-Nokia Chair of Excellence in ICT. He was a Fulbright Fellow with The City University of New York, USA, a Nokia Foundation Visiting Professor, and a Royal Academy of Engineering Distinguished Visiting Fellow. His recent research awards include the 2021 EURASIP Best Paper Award, the 2022 IEEE COMSOC Outstanding Paper Award, the 2022 Michel Monpetit Prize conferred by the French Academy of Sciences, the 2023 EURASIP Best Paper Award, the 2023 IEEE ICC Best Paper Award (wireless), the 2023 IEEE COMSOC Fred W. Ellersick Prize, the 2023 IEEE COMSOC Heinrich Hertz Award, and the 2023 IEEE VTS James Evans Avant Grade Award. He served as the Editor-in-Chief for IEEE COMMUNICATIONS LETTERS (2019–2023). He is also serving in the Advisory Board.